

LIBRARY
Michigan State
University

This is to certify that the

thesis entitled


ESTABLISHMENT OF CYLINDER KIT DESIGN GUIDELINES
FOR FOUR-STROKE INTERNAL COMBUSTION ENGINES
USING NUMERICAL SIMULATIONS

presented by

Stephen Robert Yen

has been accepted towards fulfillment
of the requirements for

M.S. degree in Mechanical Engineering


Major professor

Date 12/07/00

PLACE IN RETURN BOX to remove this checkout from your record.
TO AVOID FINES return on or before date due.
MAY BE RECALLED with earlier due date if requested.

DATE DUE	DATE DUE	DATE DUE

**ESTABLISHMENT OF CYLINDER KIT DESIGN GUIDELINES FOR
FOUR-STROKE INTERNAL COMBUSTION ENGINES USING NUMERICAL
SIMULATIONS**

By

Stephen Robert Yen

A THESIS

**Submitted to
Michigan State University
in partial fulfillment of the requirements
for the degree of
MASTER OF SCIENCE**

Department of Mechanical Engineering

2000

ABSTRACT

ESTABLISHMENT OF CYLINDER KIT DESIGN GUIDELINES FOR FOUR-STROKE INTERNAL COMBUSTION ENGINES USING NUMERICAL SIMULATIONS

By

Stephen Robert Yen

Engine efficiency and emissions performance constraints have motivated the automotive industry to focus research on piston and piston ring pack design. This thesis presents guidelines on the practical aspects of cylinder kit geometry that should be followed to achieve maximum engine performance. Theoretical explanations of why these designs provide improved performance are also discussed.

Due to the thousands of engine operating conditions that were tested, the ring-pack performance estimates could only be found by means of computer simulation. The Cylinder kit Analysis System for Engines (CASE) was utilized to obtain the results.

A simple optimizing program was initially written using finite difference methods. The results of both this program and a previously written (more advanced) optimizing program showed that the parameter values often lie on the constraints. Additional analyses were performed and the predicted results showed that many of the cylinder kit geometries (ring axial width, piston groove height, etc.) have predictable relationships to the engine performance. These relationships are analyzed in further detail in this thesis.

This thesis is dedicated to my parents

Robert Yen

&

Mei-Rong Yen

For their love, guidance and motivation

TABLE OF CONTENTS

TABLE OF CONTENTS.....	iv
LIST OF TABLES.....	vii
LIST OF FIGURES	viii
NOMENCLATURE	xiv
CHAPTER 1: INTRODUCTION.....	1
1.1 Overview.....	1
1.2 Motivation.....	2
1.2.1 Advantages Over Optimization Program.....	2
1.2.2 Advantages Over Physical Testing	3
1.3 Objectives	3
CHAPTER 2: FUNDAMENTAL GAS DYNAMICS THEORY	4
2.1 Introduction to Gas Flows in Cylinder Kits.....	4
2.2 Gas Flow Model.....	5
2.3 Energy Balance	6
2.4 Thermodynamic Gas Model	8
2.5 Mass Flow Model	8
2.6 Numerical Procedure	12
CHAPTER 3: RING DYNAMICS THEORY	15
3.1 Introduction to Ring Dynamics.....	15
3.2 Ring Forces in Axial Direction.....	15
3.2.1 Inertial Force.....	15
3.2.2 Pressure Forces	16
3.2.3 Friction Forces	16
3.3 Ring Flutter	17
3.4 Ring Collapse.....	18
CHAPTER 4: COMPUTER SIMULATION VALIDATION.....	22
4.1 Overview.....	22
4.2 Comparisons	22
4.2.1 Comparing Predicted Blowby Maps.....	22
4.2.2 Comparing Measured and Predicted Blowby Maps	22
CHAPTER 5: COMPUTER SIMULATION SETUP	24
5.1 Simulation Hardware and Software	24
5.2 Operating Conditions	25

5.3 Cylinder Kit Schematics	25
5.4 Engines Simulated	27
5.5 Gas Pressure Input Data.....	43
5.6 Ring Geometry Input Data.....	44
5.6.1 Primary Parametric Study	44
5.6.2 Secondary Parametric Study	45
5.7 Bore, Piston, and Connecting Rod Data	46
5.8 Ring Twist.....	46
 CHAPTER 6: COMPUTER SIMULATION RESULTS	49
6.1 Overview	49
6.2 Plots	49
 CHAPTER 7: COMPUTER SIMULATION ANALYSIS.....	50
7.1 Blowby Map Analysis	50
7.2 General Observations.....	51
7.2.1 Effect of Blowby Magnitude on Parameter Sensitivity	51
7.2.2 Note on Engine Comparisons	51
7.3 End Gap Analysis	52
7.3.1 Mini-Study on 5.4 L V8 Ford Motor Company Engine	53
7.3.2 Note of Caution.....	55
7.4 Axial Width Analysis.....	55
7.5 Groove Height Analysis.....	56
7.6 Small Clearance Between Top of Ring and Top of Groove	56
7.7 Radial Thickness Analysis.....	57
7.7.1 Relating Ring Wear to Radial Thickness.....	58
7.8 Groove Diameter Analysis.....	58
7.8.1 Basic Overview	58
7.8.2 Exceptions to the Rule	58
 CHAPTER 8: CONCLUSIONS AND RECOMMENDATIONS.....	60
8.1 General Implications.....	60
8.2 Top Ring Trends	60
8.3 HC Emissions	61
8.4 Top and Second Compression Ring Relation	61
8.5 Recommendations.....	61
 CHAPTER 9: REFERENCES	63
 CHAPTER 10: APPENDIX A	64
10.1 Note About Blowby Scale	64
10.2 Parametric Study Plots for Ford 2.3 L I4 Engine	64
10.2.1 Original Design.....	65
10.2.2 End Gap Variations.....	65
10.2.3 Axial Width Variations.....	68
10.2.4 Groove Height Variations.....	71

10.2.5 Radial Thickness Variations	73
10.2.6 Groove Diameter Variations	76
10.3 Parametric Study Plots for Ford 4.6 L V8 Engine	78
10.3.1 Original Design	79
10.3.2 End Gap Variations	79
10.3.3 Axial Width Variation	84
10.3.4 Groove Height Variation	87
10.3.5 Radial Thickness Variations	89
10.3.6 Groove Diameter Variations	91
10.4 Parametric Study Plots for Ford 5.4 L V8 Engine	95
10.4.1 Original Design	96
10.4.2 End Gap Variations	96
10.4.3 Axial Width Variations	100
10.4.4 Groove Height Variations	103
10.4.5 Radial Thickness Variations	108
10.4.6 Groove Diameter Variations	112
10.5 Ford 5.4 L V8 Engine Mini-Study	116

LIST OF TABLES

TABLE 1: Computer Hardware	24
TABLE 2: Computer Software	24
TABLE 3: Ford 5.4 L V8 2 Valve Cylinder Kit Specifications	28
TABLE 4: Ford 4.6 L V8 2 Valve Cylinder Kit Specifications	33
TABLE 5: Ford 2.3 L I4 2 Valve Cylinder Kit Specifications.....	38
TABLE 6: Ford 5.4 L V8 Engine Top Compression Ring Test Matrix	44
TABLE 7: Ford 4.6 L V8 Engine Top Compression Ring Test Matrix	44
TABLE 8: Ford 2.3 L I4 Engine Top Compression Ring Test Matrix.....	45
TABLE 9: Ford 5.4 L V8 Engine Top and Second Compression Ring Test Matrix.....	45
TABLE 10: Ford 5.4 L V8 Engine Top Piston Groove Test Matrix	46
TABLE 11: Ford 4.6 L V8 Engine Top Piston Groove Test Matrix	46
TABLE 12: Ford 2.3 L V8 Engine Top Piston Groove Test Matrix	46
TABLE 13: Qualitative Parametric Sensitivity	60

LIST OF FIGURES

FIGURE 1: Gas Flow Paths.....	4
FIGURE 2: Orifice-Volume Model Schematic	5
FIGURE 3: Flow Path Schematic for a Floating Ring	17
FIGURE 4: Force Balance Conditions for Ring Collapse	19
FIGURE 5: Ford 5.4 L V8 Engine Blowby Map - Measured [6]	23
FIGURE 6: Ford 5.4 L V8 Engine Blowby Map - Predicted [6].....	23
FIGURE 7: Process Flow Chart.....	25
FIGURE 8: Piston Ring Cross Section	25
FIGURE 9: Piston Ring Top View	26
FIGURE 10: Piston Ring Face Profiles	26
FIGURE 11: Three Piece Oil Ring Dimensions	26
FIGURE 12: Piston Groove Cross Section.....	27
FIGURE 13: Skirt Dimensions	27
FIGURE 14: Typical Blowby Map.....	50
FIGURE 15: Ring Motion Versus Crank Angle (Ring Collapse)	54
FIGURE 16: Aged Piston Ring and Groove with Large Clearance	57
FIGURE 17: Ring Collapse Interference.....	57
FIGURE 18: Ring Motion Versus Crank Angle (Ring Collapse) With Top Ring Dip	59
FIGURE 19: Ford 2.3 L I4 Engine Blowby Map - Original Design	65
FIGURE 20: Ford 2.3 L I4 Engine Blowby Map - 0.4 End Gap Ring 1	65
FIGURE 21: Ford 2.3 L I4 Engine Blowby Map - 0.5 End Gap Ring 1	66

FIGURE 22: Ford 2.3 L I4 Engine Blowby Map - 0.6 End Gap Ring 1	66
FIGURE 23: Ford 2.3 L I4 Engine Blowby Map - 0.7 End Gap Ring 1	67
FIGURE 24: Ford 2.3 L I4 Engine Blowby Map - 0.8 End Gap Ring 1	67
FIGURE 25: Ford 2.3 L I4 Engine Blowby Map - 0.9 End Gap Ring 1	68
FIGURE 26: Ford 2.3 L I4 Engine Blowby Map - 1.47 Axial Width Ring 1	68
FIGURE 27: Ford 2.3 L I4 Engine Blowby Map - 1.49 Axial Width Ring 1	69
FIGURE 28: Ford 2.3 L I4 Engine Blowby Map - 1.50 Axial Width Ring 1	69
FIGURE 29: Ford 2.3 L I4 Engine Blowby Map - 1.51 Axial Width Ring 1	70
FIGURE 30: Ford 2.3 L I4 Engine Blowby Map - 1.52 Axial Width Ring 1	70
FIGURE 31: Ford 2.3 L I4 Engine Blowby Map - 1.49 Groove Height Ring 1	71
FIGURE 32: Ford 2.3 L I4 Engine Blowby Map - 1.50 Groove Height Ring 1	71
FIGURE 33: Ford 2.3 L I4 Engine Blowby Map - 1.51 Groove Height Ring 1	72
FIGURE 34: Ford 2.3 L I4 Engine Blowby Map - 1.52 Groove Height Ring 1	72
FIGURE 35: Ford 2.3 L I4 Engine Blowby Map - 1.54 Groove Height Ring 1	73
FIGURE 36: Ford 2.3 L I4 Engine Blowby Map - 4.0 Radial Thickness Ring 1	73
FIGURE 37: Ford 2.3 L I4 Engine Blowby Map - 4.1 Radial Thickness Ring 1	74
FIGURE 38: Ford 2.3 L I4 Engine Blowby Map - 4.2 Radial Thickness Ring 1	74
FIGURE 39: Ford 2.3 L I4 Engine Blowby Map - 4.3 Radial Thickness Ring 1	75
FIGURE 40: Ford 2.3 L I4 Engine Blowby Map - 4.4 Radial Thickness Ring 1	75
FIGURE 41: Ford 2.3 L I4 Engine Blowby Map - 87.10 Groove Diameter Ring 1	76
FIGURE 42: Ford 2.3 L I4 Engine Blowby Map - 87.30 Groove Diameter Ring 1	76
FIGURE 43: Ford 2.3 L I4 Engine Blowby Map - 87.50 Groove Diameter Ring 1	77
FIGURE 44: Ford 2.3 L I4 Engine Blowby Map - 87.70 Groove Diameter Ring 1	77

FIGURE 45: Ford 2.3 L I4 Engine Blowby Map - 87.90 Groove Diameter Ring 1	78
FIGURE 46: Ford 4.6 L V8 Engine Blowby Map - Original Design.....	79
FIGURE 47: Ford 4.6 L V8 Engine Blowby Map - 0.4 End Gap Ring 1	79
FIGURE 48: Ford 4.6 L V8 Engine Blowby Map - 0.5 End Gap Ring 1	80
FIGURE 49: Ford 4.6 L V8 Engine Blowby Map - 0.6 End Gap Ring 1	80
FIGURE 50: Ford 4.6 L V8 Engine Blowby Map - 0.7 End Gap Ring 1	81
FIGURE 51: Ford 4.6 L V8 Engine Blowby Map - 0.8 End Gap Ring 1	81
FIGURE 52: Ford 4.6 L V8 Engine Blowby Map - 0.9 End Gap Ring 1	82
FIGURE 53: Ford 4.6 L V8 Engine Blowby Map - 1.0 End Gap Ring 1	82
FIGURE 54: Ford 4.6 L V8 Engine Blowby Map - 1.1 End Gap Ring 1	83
FIGURE 55: Ford 4.6 L V8 Engine Blowby Map - 1.2 End Gap Ring 1	83
FIGURE 56: Ford 4.6 L V8 Engine Blowby Map - 1.3 End Gap Ring 1	84
FIGURE 57: Ford 4.6 L V8 Engine Blowby Map - 1.48 Axial Width Ring 1.....	84
FIGURE 58: Ford 4.6 L V8 Engine Blowby Map - 1.49 Axial Width Ring 1.....	85
FIGURE 59: Ford 4.6 L V8 Engine Blowby Map - 1.50 Axial Width Ring 1.....	85
FIGURE 60: Ford 4.6 L V8 Engine Blowby Map - 1.51 Axial Width Ring 1.....	86
FIGURE 61: Ford 4.6 L V8 Engine Blowby Map - 1.52 Axial Width Ring 1.....	86
FIGURE 62: Ford 4.6 L V8 Engine Blowby Map - 1.48 Groove Height Ring 1.....	87
FIGURE 63: Ford 4.6 L V8 Engine Blowby Map - 1.49 Groove Height Ring 1.....	87
FIGURE 64: Ford 4.6 L V8 Engine Blowby Map - 1.50 Groove Height Ring 1.....	88
FIGURE 65: Ford 4.6 L V8 Engine Blowby Map - 1.51 Groove Height Ring 1.....	88
FIGURE 66: Ford 4.6 L V8 Engine Blowby Map - 1.52 Groove Height Ring 1.....	89
FIGURE 67: Ford 4.6 L V8 Engine Blowby Map - 4.1 Radial Thickness Ring 1	89

FIGURE 68: Ford 4.6 L V8 Engine Blowby Map - 4.3 Radial Thickness Ring 1	90
FIGURE 69: Ford 4.6 L V8 Engine Blowby Map - 4.5 Radial Thickness Ring 1	90
FIGURE 70: Ford 4.6 L V8 Engine Blowby Map - 4.7 Radial Thickness Ring 1	91
FIGURE 71: Ford 4.6 L V8 Engine Blowby Map - 80.91 Groove Diameter Ring 1	91
FIGURE 72: Ford 4.6 L V8 Engine Blowby Map - 81.11 Groove Diameter Ring 1	92
FIGURE 73: Ford 4.6 L V8 Engine Blowby Map - 81.31 Groove Diameter Ring 1	92
FIGURE 74: Ford 4.6 L V8 Engine Blowby Map - 81.51 Groove Diameter Ring 1	93
FIGURE 75: Ford 4.6 L V8 Engine Blowby Map - 81.71 Groove Diameter Ring 1	93
FIGURE 76: Ford 4.6 L V8 Engine Blowby Map - 81.91 Groove Diameter Ring 1	94
FIGURE 77: Ford 4.6 L V8 Engine Blowby Map - 82.11 Groove Diameter Ring 1	94
FIGURE 78: Ford 4.6 L V8 Engine Blowby Map - 82.20 Groove Diameter Ring 1	95
FIGURE 79: Ford 5.4 L V8 Engine Blowby Map - Original Design.....	96
FIGURE 80: Ford 5.4 L V8 Engine Blowby Map - 0.3 End Gap Ring 1	96
FIGURE 81: Ford 5.4 L V8 Engine Blowby Map - 0.4 End Gap Ring 1	97
FIGURE 82: Ford 5.4 L V8 Engine Blowby Map - 0.5 End Gap Ring 1	97
FIGURE 83: Ford 5.4 L V8 Engine Blowby Map - 0.6 End Gap Ring 1	98
FIGURE 84: Ford 5.4 L V8 Engine Blowby Map - 0.7 End Gap Ring 1	98
FIGURE 85: Ford 5.4 L V8 Engine Blowby Map - 0.8 End Gap Ring 1	99
FIGURE 86: Ford 5.4 L V8 Engine Blowby Map - 0.9 End Gap Ring 1	99
FIGURE 87: Ford 5.4 L V8 Engine Blowby Map - 1.46 Axial Width Ring 1	100
FIGURE 88: Ford 5.4 L V8 Engine Blowby Map - 1.47 Axial Width Ring 1	100
FIGURE 89: Ford 5.4 L V8 Engine Blowby Map - 1.48 Axial Width Ring 1	101
FIGURE 90: Ford 5.4 L V8 Engine Blowby Map - 1.49 Axial Width Ring 1	101

FIGURE 91: Ford 5.4 L V8 Engine Blowby Map - 1.50 Axial Width Ring 1.....	102
FIGURE 92: Ford 5.4 L V8 Engine Blowby Map - 1.51 Axial Width Ring 1.....	102
FIGURE 93: Ford 5.4 L V8 Engine Blowby Map - 1.52 Axial Width Ring 1.....	103
FIGURE 94: Ford 5.4 L V8 Engine Blowby Map - 1.46 Groove Height Ring 1.....	103
FIGURE 95: Ford 5.4 L V8 Engine Blowby Map - 1.47 Groove Height Ring 1.....	104
FIGURE 96: Ford 5.4 L V8 Engine Blowby Map - 1.48 Groove Height Ring 1.....	104
FIGURE 97: Ford 5.4 L V8 Engine Blowby Map - 1.49 Groove Height Ring 1.....	105
FIGURE 98: Ford 5.4 L V8 Engine Blowby Map - 1.50 Groove Height Ring 1.....	105
FIGURE 99: Ford 5.4 L V8 Engine Blowby Map - 1.51 Groove Height Ring 1.....	106
FIGURE 100: Ford 5.4 L V8 Engine Blowby Map - 1.52 Groove Height Ring 1.....	106
FIGURE 101: Ford 5.4 L V8 Engine Blowby Map - 1.54 Groove Height Ring 1.....	107
FIGURE 102: Ford 5.4 L V8 Engine Blowby Map - 1.55 Groove Height Ring 1.....	107
FIGURE 103: Ford 5.4 L V8 Engine Blowby Map - 3.2 Radial Thickness Ring 1	108
FIGURE 104: Ford 5.4 L V8 Engine Blowby Map - 3.3 Radial Thickness Ring 1	108
FIGURE 105: Ford 5.4 L V8 Engine Blowby Map - 3.4 Radial Thickness Ring 1	109
FIGURE 106: Ford 5.4 L V8 Engine Blowby Map - 3.5 Radial Thickness Ring 1	109
FIGURE 107: Ford 5.4 L V8 Engine Blowby Map - 3.6 Radial Thickness Ring 1	110
FIGURE 108: Ford 5.4 L V8 Engine Blowby Map - 3.7 Radial Thickness Ring 1	110
FIGURE 109: Ford 5.4 L V8 Engine Blowby Map - 3.8 Radial Thickness Ring 1	111
FIGURE 110: Ford 5.4 L V8 Engine Blowby Map - 3.9 Radial Thickness Ring 1	111
FIGURE 111: Ford 5.4 L V8 Engine Blowby Map - 4.0 Radial Thickness Ring 1	112
FIGURE 112: Ford 5.4 L V8 Engine Blowby Map - 82.00 Groove Diameter Ring 1....	112
FIGURE 113: Ford 5.4 L V8 Engine Blowby Map - 82.40 Groove Diameter Ring 1....	113

FIGURE 114: Ford 5.4 L V8 Engine Blowby Map - 82.60 Groove Diameter Ring 1....	113
FIGURE 115: Ford 5.4 L V8 Engine Blowby Map - 82.60 Groove Diameter Ring 1....	114
FIGURE 116: Ford 5.4 L V8 Engine Blowby Map - 82.80 Groove Diameter Ring 1....	114
FIGURE 117: Ford 5.4 L V8 Engine Blowby Map - 83.00 Groove Diameter Ring 1....	115
FIGURE 118: Ford 5.4 L V8 Engine Blowby Map - 83.20 Groove Diameter Ring 1....	115
FIGURE 119: Ford 5.4 L V8 Engine Blowby Map - 0.3 End Gap Ring 1 & 2	116
FIGURE 120: Ford 5.4 L V8 Engine Blowby Map - 0.4 End Gap Ring 1 & 2	116
FIGURE 121: Ford 5.4 L V8 Engine Blowby Map - 0.4 End Gap Ring 1 & 2	117
FIGURE 122: Ford 5.4 L V8 Engine Blowby Map - 0.5 End Gap Ring 1 & 2	117
FIGURE 123: Ford 5.4 L V8 Engine Blowby Map - 0.6 End Gap Ring 1 & 2	118
FIGURE 124: Ford 5.4 L V8 Engine Blowby Map - 0.7 End Gap Ring 1 & 2	118
FIGURE 125: Ford 5.4 L V8 Engine Blowby Map - 0.8 End Gap Ring 1 & 2	119
FIGURE 126: Ford 5.4 L V8 Engine Blowby Map - 0.9 End Gap Ring 1 & 2	119

NOMENCLATURE

English Symbols

Name	Definition	Units
a	Axial acceleration of the ring	$\frac{\text{m}^2}{\text{sec}}$
A	Area pressure force acts on	m^2
A_{bore}	Maximum bore area	m^2
A_{max}	Maximum flow area	m^2
A_N	Flow area for ring N	m^2
$A_{pouterface}$	Area of outer ring face	m^2
$A_{pinnerface}$	Area of inner ring face	m^2
A_{ring}	Area occupied by the ring	m^2
c_v	Specific heat at constant volume	$\frac{\text{J}}{\text{kg/K}}$
d	Inner surface diameter on which pressure force acts	m
D	Bore diameter	m
D_{eff}	Effective ring outer diameter	m
E	Modulus of elasticity	Pa
F_F	Friction force	N

F_I	Inertial force	N
F_P	Pressure force	N
$F_{tension}$	Ring tension force	N
F_T	Ring tension force	N
I	Moment of Inertia	m ⁴
K_c	Orifice discharge coefficient	unitless
K_i	Blowby parameter	$\frac{K^{1/2}}{\text{Pa} - \text{radians}}$
m	Mass	kg
\dot{m}	Mass flow rate	$\frac{\text{kg}}{\text{sec}}$
m_N^*	Non-dimensionalized mass flow rate for ring N	unitless
p	Pressure behind ring	Pa
p_{eff}	Effective ring perimeter	m
P	Pressure	Pa
P^*	Non-dimensionalized pressure	unitless
P_{atm}	Atmospheric pressure	Pa
P_c	Critical pressure	Pa
P_{groove}	Pressure behind ring groove	Pa
P_N	Pressure above ring N	Pa

R	Gas constant for air	$\frac{\text{J}}{\text{kg/K}}$
S_N	Distance of flow	m
t	Time	sec
t_{ax}	Axial width of ring	m
T	Temperature	K
T^*	Non-dimensionalized temperature	K
T_c	Combustion chamber temperature	K
T_N	Temperature above ring N	K
u_N	Internal energy of gas at ring N	J
v_{ax}	Axial velocity of ring	$\frac{\text{m}}{\text{sec}}$
v_c	Critical flow velocity	$\frac{\text{m}}{\text{sec}}$
v_N	Velocity of the gas flowing past ring N	$\frac{\text{m}}{\text{sec}}$
V_N	Volume below ring N	m^3
x_{endgap}	End gap clearance	m

Greek Symbols

Name	Definition	Units
δ_r	radial displacement	m
γ	Specific heat ratio	unitless

μ	Kinematic coefficient friction	unitless
ω	Angular crankshaft velocity	$\frac{\text{radians}}{\text{sec}}$
π	Pi	unitless
ρ_N	Density of flow at ring N	$\frac{\text{kg}}{\text{m}^3}$
θ	Crank angle position	radians

Acronyms and Abbreviations

Name	Definition
CASE	Cylinder kit Analysis System for Engines
ENGSIM	Engine Simulation
GESIM	General Engine Simulation
HC	Hydrocarbon
WOT	Wide Open Throttle

CHAPTER 1. INTRODUCTION

1.1 Overview

The primary function of piston rings is to provide a moveable seal in a cylinder kit to prevent combustion gases from moving past the piston. Blowby is defined in this thesis as the sum of the gases that flows past the top piston ring either towards the crankcase (foreflow) or back into the combustion chamber (backflow). Foreflow “...decreases horsepower, decreased engine torque, increases oil contamination, [and] decreases engine life...” [1] Backflow increases hydrocarbon emissions and increases oil consumption. More specifically, “... piston ring pack crevices [are] responsible for 80% of the total HC returning from the crevices to the cylinder after combustion. [2] In order for an engine to perform desirably, piston rings must be designed specially to function with a particular cylinder kit.

One of the great challenges automotive engineers face in cylinder kit design today is the large number of operating conditions for which the designs must perform. In the past, testing a design for 10 loads and 10 engine speeds would require 100 measurements with consistent setups. Often measurements or computer predictions in previous studies would be made fixed at full or minimal load conditions for a few engine speeds [3]. However, as shown later in this thesis, cylinder kit performance can vary a great deal depending upon the operating conditions.

Due to recent computer advancements, software has been developed at Michigan State University to predict cylinder kit performance for over 100 operating conditions within minutes. This program, the Cylinder kit Analysis System for Engines

(CASE), has made it possible to perform a parametric study for a large set of operating conditions.

A blowby optimization (minimization) program was originally developed to try to find the optimal piston ring axial thickness, and piston ring end gap. After running the optimization for four different engines at several operating conditions, it was found that both the axial thickness, and the end gap often ended up at the design constraints. The parameter predictions that did not lie at the constraints showed an insignificant influence on the blowby performance. Such an observation would suggest that perhaps there existed a “proportional” relationship between blowby and certain cylinder kit design parameters.

1.2 Motivation

Discovering the direct relationships between blowby and various ring geometric parameters would significantly reduce both initial design and redesign times. Understanding the behavior of blowby performance as simple cause and effect relationships is currently more time efficient than producing a sophisticated cylinder kit optimization program.

1.2.1 Advantages Over Optimization Program

There are several complications in producing a useful optimization program. The coupled equations approximating ring behavior are difficult and too computationally intensive to solve semi-analytically for more than a couple of design variables simultaneously. Purely numerical methods utilizing ring pack modeling programs as a black box to obtain blowby values, require that the black box be executed several thousands of times due to the scores of operating points in which an engine runs. Even with some of the fastest operating black boxes taking approximately three seconds per run,

several days of optimization may be required to find a local optimum point—not even a global optimum point. To find the global optimum point, several optimizations would have to be run at different initial design parameter guesses. In other words, computing technology and creative optimization techniques will require significant development before optimization programs will be worthwhile in determining ideal cylinder kit geometries.

1.2.2 Advantages Over Physical Testing

Besides saving on cost and time (by not producing custom piston rings), using a numerical simulation for the study had other beneficial aspects over physical testing. “Generally only the gas flowing into the crankcase can be measured.” [4] Accounting for the blowby flowing (backflow) into the combustion chamber is important since it strongly affects hydrocarbon emissions. Furthermore, problems associated with running an engine at high RPMs and WOT for long periods of time are avoided.

1.3 Objectives

The objective of the study in the thesis was to determine the influences on blowby due to the following design parameters: end gap clearance, axial width, groove height, radial thickness, and groove diameter. Ford 5.4 L, 4.6 L, and 2.3 L four-stroke gasoline engines were simulated in the study. Engine loads ranged from idling (0%) to maximum engine load (100%) in ~8.333% increments, and from 1000 to 5000 RPM in 500 RPM increments. Further details of the experiment step is documented in Heading 5.1.

CHAPTER 2. FUNDAMENTAL GAS DYNAMICS THEORY

2.1 Introduction to Gas Flows in Cylinder Kits

Combustion gases flow through piston ring packs due to differences in pressures above and below piston rings. The gases usually flow through the end gaps, the clearance between the ring top and its respective groove top, and the clearance between the ring bottom and its respective groove bottom.

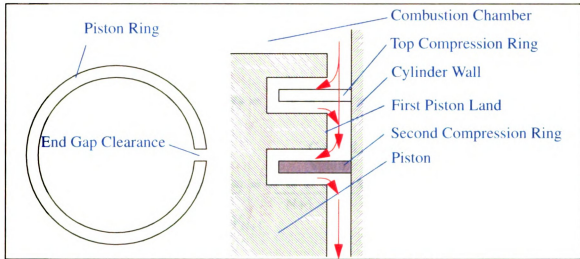


Figure 1: Gas Flow Paths

Engine designers must consider several issues. End gap areas gradually increase due to ring wear. [5] Sometimes a consequence of increased end gap clearances, there is a phenomenon called piston ring collapse in which large amounts of combustion gases can flow across the piston ring face. [6] Gases can also travel across the ring face in the case of severe bore distortion. Under such circumstances, almost all of the oil is removed from the liner at the points of contact, causing rapid wear and possibly seizure. These above are examples of some problems, that need to be addressed when designing an cylinder kit. Many of these problems can be solved with well-designed models.

2.2 Gas Flow Model

The orifice-volume model is used in the Cylinder kit Analysis System for Engines (CASE) to determine the gas flow through the end gaps and the radial clearance between the piston groove and the piston ring. These “orifices” are assumed to be square-edged. As shown in Figure 2, the volumes are the spaces enclosed by the rings adjacent to the piston lands, and the space formed by the internal grooves and the respective inner surface piston rings surfaces.

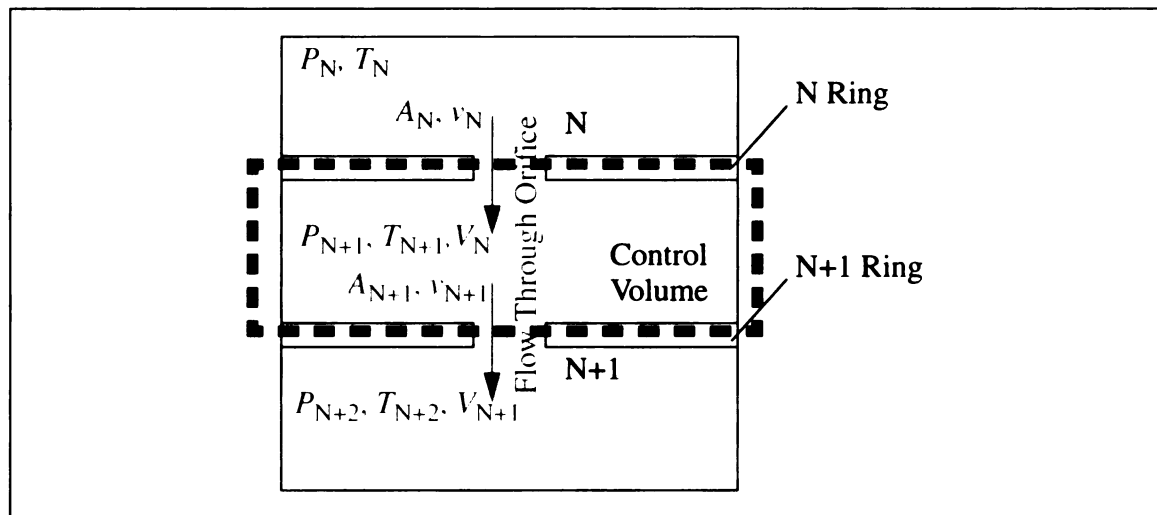


Figure 2: Orifice-Volume Model Schematic

In the orifice-volume model used, gas flow calculations are one-dimensional. As the gas flows through the ring pack, it assumes the temperature of the adjacent piston land. The temperature of the piston lands are assumed to be constant with respect to time. The gas flow through the ring pack is highly dependent on the gas discharge coefficient. Yun, Chun, and Lee [7] found that discharge coefficients of 0.83 overestimate the inter-ring gas pressures. According to Heywood [8] and previous tests with Ford and Daimler Chrysler, analyses (with the CASE system) indicated that 0.65 was an appropriate selection for the discharge coefficient for a gasoline engine.

The calculations of the inter-ring gas pressures are found using an iterative process. Initially, a guess of the inter-ring gas pressure is made. The mass flow rates are calculated using this guess. Utilizing these mass flow rates, a new set of inter-ring gas pressures are calculated and compared to the original guess. If the guess does not match the new set of inter-ring gas pressures, the process is repeated using the new pressures as the guess.

Although the CASE system supports piston tilt analysis, piston tilt was omitted from the study for simplicity and time savings. According to Truscott, Reid and Ruddy [9], the piston tilt's effect on gas flows is negligible in both measured and simulated studies.

2.3 Energy Balance

The following energy analysis will consider a steady gas flow through a control volume, as shown in Figure 2. All gases entering from 1 must exit through 2, due to the steady flow assumption. Since the heat transfer rate is very small, the flow is considered to be adiabatic. The Reynolds number in inter-ring gas flows are sufficiently high, such that viscous effects can be neglected; the flow is isentropic. The work done in the control

volume by the gas is assumed to be negligible. [5] However, there is assumed to be flow work at the inlet and exit of the control volume. They are given as follows:

$$\begin{aligned}
 \text{Inlet Flow Work} &= \frac{\text{Force} \times \text{Distance}}{\text{Mass}} \\
 &= \frac{P_N A_N \times S_N}{m} \\
 &= P_N A_N \times \frac{1}{A_N \rho_N} \\
 &= \frac{P_N}{\rho_N}
 \end{aligned} \tag{1}$$

$$\begin{aligned}
 \text{Exit Flow Work} &= \frac{\text{Force} \times \text{Distance}}{\text{Mass}} \\
 &= \frac{P_{N+1} A_{N+1} \times S_{N+1}}{m} \\
 &= P_{N+1} A_{N+1} \times \frac{1}{A_{N+1} \rho_{N+1}} \\
 &= \frac{P_{N+1}}{\rho_{N+1}}
 \end{aligned} \tag{2}$$

where P is pressure, A is flow area, S is distance, m is mass and ρ is gas density. The subscript N represents the control volume inlet, while the subscript $N + 1$ represents the control volume exit.

Since the control volume is relatively small, gravitational potential energy effects are negligible. The internal energies and velocities at the inlet and exit of the control volume are significant and are thus included in the final energy balance equation.

The final energy balance energy equation per unit mass is given as

$$\frac{P_N}{\rho_N} - \frac{P_{N+1}}{\rho_{N+1}} = u_{N+1} - u_N + \frac{v_{N+1}^2 - v_N^2}{2} \tag{3}$$

where u is the internal energy of the gas and v is the velocity of the gas.

2.4 Thermodynamic Gas Model

The high temperatures present in combustion gases allows the ideal gas law equation of state to be used with relatively insignificant error. This equation of state is

$$P = \rho RT \quad (4)$$

where P is the absolute pressure, ρ is the gas density, R is the gas constant for air and T is the temperature on an absolute scale.

From the assumption that the flow is isentropic, and the ideal gas relations, it can be shown then that

$$\frac{P_N}{P_{N+1}} = \left(\frac{\rho_{N+1}}{\rho_N} \right)^\gamma = \left(\frac{T_N}{T_{N+1}} \right)^{\frac{\gamma}{\gamma-1}} \quad (5)$$

where γ is the specific heat ratio.

2.5 Mass Flow Model

The one-dimensional continuity equation is

$$\rho_N A_N v_N = \rho_{N+1} A_{N+1} v_{N+1} = \dot{m} = \frac{dm}{dt} \quad (6)$$

where \dot{m} is mass flow rate, m is mass and t is time.

Knowing that the $u_{N+1} - u_N$ in Equation (3) can be replaced by

$$u_{N+1} - u_N = c_v(T_{N+1} - T_N) \quad (7)$$

where c_v is the specific heat at constant volume, Equation (3) can be solved for velocity of the orifice flow. If v_N is set to zero, the relative exiting velocity (v_{N+1}) can be given by

$$v_{N+1} = \sqrt{2\left(\left(\frac{P_N}{\rho_N} - \frac{P_{N+1}}{\rho_{N+1}}\right) + c_v(T_N - T_{N+1})\right)} \quad (8)$$

c_v in Equation (8) can be replaced knowing

$$c_v = \frac{R}{\gamma - 1} \quad (9)$$

thus giving

$$v_{N+1} = \sqrt{\left(\frac{2\gamma}{\gamma - 1}\right)\left(\frac{P_N}{\rho_N} - \frac{P_{N+1}}{\rho_{N+1}}\right)} \quad (10)$$

By using the isentropic relations given in Equation (5), terms in Equation (10) can be replaced as shown in Equation (11) and Equation (12).

$$\left(\frac{P_N}{\rho_N} - \frac{P_{N+1}}{\rho_{N+1}}\right) = \frac{P_N}{\rho_N} \left(1 - \left(\frac{P_{N+1}}{P_N}\right)^{\frac{(\gamma-1)}{\gamma}}\right) \quad (11)$$

$$v_{N+1} = \sqrt{\left(\frac{2\gamma}{\gamma - 1}\right) \frac{P_N}{\rho_N} \left(1 - \left(\frac{P_{N+1}}{P_N}\right)^{\frac{(\gamma-1)}{\gamma}}\right)} \quad (12)$$

Using Equation (4), Equation (5), Equation (6), and Equation (12), the following mass flow rate equation can be developed:

$$\dot{m} = A_{N+1} \sqrt{\frac{2\gamma\rho_N P_N}{\gamma - 1} \left(\left(\frac{P_{N+1}}{P_N}\right)^{\frac{2}{\gamma}} - \left(\frac{P_{N+1}}{P_N}\right)^{\frac{\gamma+1}{\gamma}} \right)} \quad (13)$$

Equation (13) clearly shows that if mass flow rate is plotted against the pressure ratio $\frac{P_{N+1}}{P_N}$ that mass flow rate is parabolic. However, due to a choked flow phenomenon, Equation (13) applies only for a pressure ratio greater than the critical pressure ratio. This critical pressure ratio is found by differentiating Equation (13) with respect to P_{N+1} , setting $\frac{d\dot{m}}{dP_{N+1}}$ equal to zero and solving for P_{N+1} . Performing these operations yields

$$P_{N+1} \Big|_{\frac{d\dot{m}}{dP_{N+1}} = 0} = P_c = P_N \left(\frac{2}{\gamma + 1} \right)^{\frac{\gamma}{\gamma - 1}} \quad (14)$$

where P_c is the critical pressure.

Since for combustion gases γ is approximately 1.3, that would mean that the critical pressure ratio is

$$\frac{P_c}{P_N} = 0.546 \quad (15)$$

The fluid velocity for pressure ratios below the critical pressure ratio can be found by inserting the critical pressure into Equation (12). Thus, the choked flow velocity (v_c) is

$$v_c = \sqrt{\left(\frac{2\gamma}{\gamma - 1} \right) \frac{P_N}{\rho_c} \left(1 - \left(\frac{P_c}{P_N} \right)^{\frac{(\gamma - 1)}{\gamma}} \right)} \quad (16)$$

where ρ_c is the density at critical pressure.

Using Equation (5) and Equation (14), Equation (16) can be simplified to

$$v_c = \sqrt{\frac{\gamma P_c}{\rho_c}} \quad (17)$$

Equation (17) shows that the choked flow velocity is equal to that of the velocity of sound. Therefore, the calculations are shown to be consistent to the Mach number characteristic of choked flows. [10]

However, the theoretical mass flow rate calculated above is greater than that of the actual flow. This difference is attributed to frictional losses and streamline convergence. The coefficient of velocity and coefficient of convergence correct the theoretical model for the two respective losses. These two coefficients are multiplied together to form the orifice discharge coefficient. As mentioned earlier, for gasoline engines the orifice discharge coefficient is 0.65. So

$$\dot{m}_{actual} = K_c \dot{m}_{theoretical} \quad (18)$$

where K_c is the orifice discharge coefficient.

While now it has been shown that mass flow varies with pressure, pressure also varies with mass flow rate. Consider the ideal gas equation of state written in terms of mass instead of volume—refer to Figure 2 for subscript definitions.

$$P_{N+1} = \frac{RT_{N+1}}{V_N} m_N \quad (19)$$

Solving Equation (19) for a time, Δt , after the initial time, t , the change in pressure can be defined as

$$P_{N+1} + \Delta P_{N+1} = \frac{RT_{N+1}}{V_N} (m_N + \dot{m}_N \Delta t - \dot{m}_{N+1} \Delta t) \quad (20)$$

Letting Δt approach zero, Equation (20) becomes

$$\frac{dP_{N+1}}{dt} = \frac{RT_{N+1}}{V_N}(\dot{m}_N - \dot{m}_{N+1}) \quad (21)$$

2.6 Numerical Procedure

Calculating mass flow rates using a numerical procedure first requires that the variables in the equations used are non-dimensionalized. Omitting this non-dimensionalization step often leads to having numerical stability problems.

Inter-ring gas pressure is non-dimensionalized by

$$P^* = \frac{P}{P_{atm}} \quad (22)$$

where P_{atm} is the atmospheric pressure.

Temperature is non-dimensionalized by

$$T^* = \frac{T}{T_c} \quad (23)$$

where T_c is the combustion chamber temperature.

Mass can be non-dimensionalized using

$$m^* = \frac{m}{\left(\frac{V_1 P_{atm}}{RT_c}\right)} \quad (24)$$

where V_1 is the volume between the first and second compression rings.

In order to make Equation (13) more applicable to engine studies, time (t) is replaced using

$$t = \frac{\theta}{\omega} \quad (25)$$

where θ is the crank angle, and ω is the engine speed in radians per second.

$$\frac{dm_N^*}{d\theta} = \frac{K_c A_1}{V_1 \omega} \sqrt{\frac{2\gamma R T_c}{(\gamma-1)}} \left(\frac{A_N}{A_1}\right) \left(\frac{P_N^*}{\sqrt{T_N^*}}\right) \left(\frac{P_{N+1}^*}{P_N^*}\right)^{1/\gamma} \sqrt{1 - \left(\frac{P_{N+1}^*}{P_N^*}\right)^{\frac{\gamma-1}{\gamma}}} \quad (26)$$

Since the first two fractions on the left-side of Equation (26) are constant with respect to crank angle, they can be factored out. These fractions combined are called the blowby parameter, K_i .

$$K_i = \frac{K_c A_1}{V_1 \omega} \sqrt{\frac{2\gamma R T_c}{(\gamma-1)}} \quad (27)$$

Thus, Equation (26) can be rewritten in shorter form as

$$\frac{dm_N^*}{d\theta} = K_i \left(\frac{A_N}{A_1}\right) \left(\frac{P_N^*}{\sqrt{T_N^*}}\right) \left(\frac{P_{N+1}^*}{P_N^*}\right)^{1/\gamma} \sqrt{1 - \left(\frac{P_{N+1}^*}{P_N^*}\right)^{\frac{\gamma-1}{\gamma}}} \quad (28)$$

For backflow (flow towards the combustion chamber), the mass flow equation can be given as

$$\frac{dm_N^*}{d\theta} = -K_i \left(\frac{A_N}{A_1}\right) \left(\frac{P_{N+1}^*}{\sqrt{T_{N+1}^*}}\right) \left(\frac{P_N^*}{P_{N+1}^*}\right)^{1/\gamma} \sqrt{1 - \left(\frac{P_N^*}{P_{N+1}^*}\right)^{\frac{\gamma-1}{\gamma}}} \quad (29)$$

The choked flow phenomenon described in Heading 2.5 must be taken into consideration for Equation (28) and Equation (29). For foreflow (flow towards the

crankcase) Equation (30) describes the maximum flow rate that can occur regardless of pressure ratio.

$$\left(\frac{dm_N^*}{d\theta}\right)\bigg|_{choked} = 0.227K_i\left(\frac{A_N}{A_1}\right)\left(\frac{P_N^*}{\sqrt{T_N^*}}\right) \quad (30)$$

The maximum backflow that can occur is given by

$$\left(\frac{dm_N^*}{d\theta}\right)\bigg|_{choked} = -0.227K_i\left(\frac{A_N}{A_1}\right)\left(\frac{P_{N+1}^*}{\sqrt{T_{N+1}^*}}\right)$$

The rate at which pressure changes due to mass flow should also be non-dimensionalized to avoid numerical stability problems. Non-dimensionalizing Equation (21) yields

$$\frac{dP_N^*}{d\theta} = T_{N+1}^*\left(\frac{V_1}{V_N}\right)(\dot{m}_N^* - \dot{m}_{N+1}^*) \quad (31)$$

CHAPTER 3. RING DYNAMICS THEORY

3.1 Introduction to Ring Dynamics

The forces that act on piston rings can be divided into the following two categories: axial forces and radial forces. The axial position of the piston ring at different stages of the engine cycle are determined by axial forces. Radial forces determine whether or not a piston ring collapses inward.

3.2 Ring Forces in Axial Direction

There are three primary forces that influence piston ring dynamics. The two other lesser forces, lubricant squeeze force and lubricant adhesive force, are relatively insignificant. The three primary forces include inertia, pressure, and friction. The relative effects of these forces on piston rings are highly dependent on the operating conditions. At high engine speeds and low engine loads, inertial forces become more dominant than the pressure forces. The opposite is also true; pressure forces are more dominant than inertial forces at lower engine speeds and high engine loads. Frictional forces even at low engine speeds and low loads, do not influence ring motion very much.

3.2.1 Inertial Force

The inertial force, F_I , can be given simply as

$$F_I = -ma \quad (32)$$

where m is the mass of the ring and a is the axial acceleration of the ring. If the ring is in contact with the piston groove, the ring's axial acceleration is the same as the piston. Pressure and friction forces determine the ring's acceleration if the ring is floating in the piston groove.

3.2.2 Pressure Forces

The pressure forces, F_P , acting on the bottom and top of the piston rings can be modeled with

$$F_P = P(r)A \quad (33)$$

where $P(r)$ is the pressure magnitude as a function of varying with radius, and A is the ring's surface area in which the pressure acts. It was assumed that the pressure dropped linearly from the outer to inner ring surface. The details of the pressure calculations are shown in Equation (31).

The area affected by the pressure is

$$A = \pi(D^2 - d^2) \quad (34)$$

where D is the bore diameter, and d varies depending upon the position of the ring. If the ring is seated at the bottom of its groove, d is the bore diameter minus two times the ring width. If the ring is touching the top of its groove, d is the piston land diameter.

3.2.3 Friction Forces

The friction forces, F_F , between the piston's ring face and cylinder liner can be approximated by the semi-empirical equation

$$F_F = (p(\pi D t_{ax}) + F_T) \left(4.8 \sqrt{\frac{\mu v_{ax}}{p}} \right) \quad (35)$$

where p is the pressure behind the ring, t_{ax} is the axial width of the ring, F_T is the force due to ring tension, μ is the kinematic coefficient of friction, and v_{ax} is the ring's axial velocity. [5]

3.3 Ring Flutter

Although the relative magnitude of the friction force is much less than either the pressure forces and inertial forces, it becomes an important factor when the pressure and inertial forces are nearly equal. When pressure and inertial forces on a piston ring are close in magnitude, the piston ring will have a tendency to quickly oscillate axially in its groove.

This “fluttering” motion occurs because the pressure and inertial forces continually alternate dominance as the gas flow paths change due to the ring motion. In the instance in which ring flutter occurs near the end of the compression stroke, inertial and pressure forces move the ring to the top of its groove. As the ring moves to the top of its groove, it is floating and thus a flow path is opened between the ring bottom and the groove bottom. As the ring reaches the top of its groove, the increasing pressure forces at

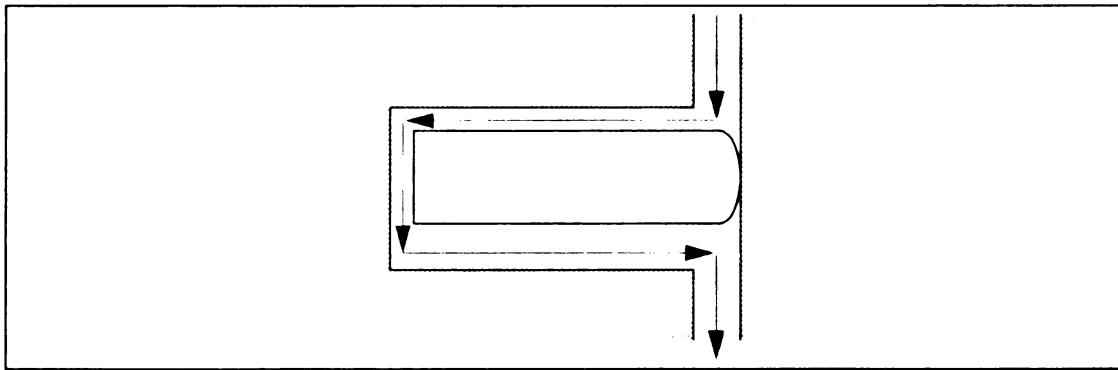


Figure 3: Flow Path Schematic for a Floating Ring

the end of the compression stroke push the ring back down. Before the ring is properly seated at the bottom of its groove. Gases can pass behind the floating ring's groove equalizing the pressure above and below the ring. The inertial force then causes the ring to return to the top of the groove. This motion can then repeat itself, impairing the ring's sealing objective.

While engine designers strive to reduce friction as much as possible, friction actually acts beneficially during the presence of conditions favorable to ring flutter. Since friction forces oppose any ring motion, they dampen these ring flutter oscillations and help to inhibit conditions that would initiate the phenomenon. Although friction causes piston ring and cylinder liner wear, its very limited presence improves ring stability.

In some instances, ring flutter can be a contributing factor to another unwanted ring behavior called ring collapse. Ring flutter also is sometimes the result of ring collapse and is an indication that ring collapse is likely to be present. Ring collapse is explained in detail in Heading 3.4.

3.4 Ring Collapse

Ring collapse is an undesirable phenomenon in which the piston ring moves radially. That is, the ring face separates from the cylinder wall creating a large area in which combustion gases can easily flow past. Ring collapse is much more detrimental to blowby performance than ring flutter.

This condition occurs when the forces acting on the ring face exceed the combined forces of the ring tension and the gas pressure behind the ring. Conditions favorable for ring collapse usually coincide with high engine speeds and low engine load. These operating conditions cause a piston ring to seat at the top of its piston groove near the end of a compression stroke; the high inertial forces (due to the high engine speed) combined with the relatively low pressure forces (due to the low engine load) keep the ring from seating on the bottom of its groove. It is undesirable to have the piston ring seated at the top of its groove since, that means the pressure gases below the ring (which are lower in magnitude than the pressure of the gases above the ring) are supporting the

ring radially. Thus, the pressure force applied to the ring face, could overcome the ring tension and gas pressure exerted from behind the ring. A force balance diagram for a scenario favoring ring collapse is shown in Figure 4.

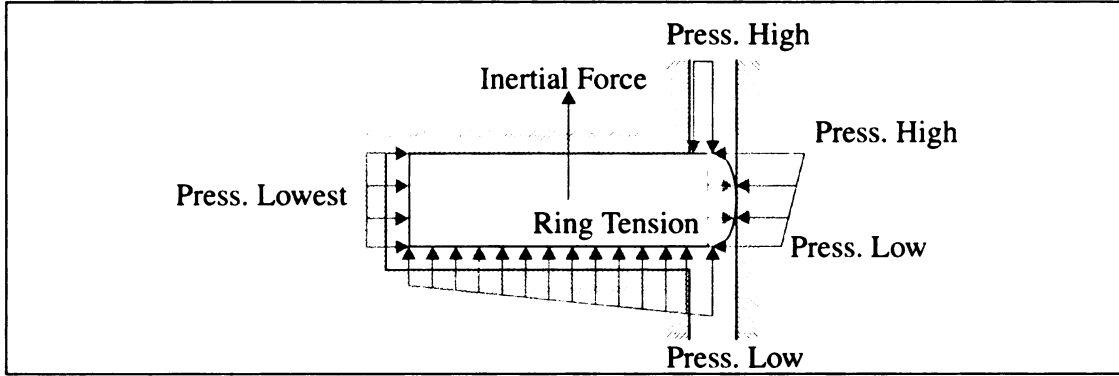


Figure 4: Force Balance Conditions for Ring Collapse

In Figure 4 ring tension is shown to be the smallest force in the force diagram. Ring tension is on the order of 25 Newtons of force for automotive gasoline engines. Whereas, the pressure force behind the top compression ring (Press. Lowest in Figure 4) can be around 200 Newtons for a standard gasoline engine under ring collapse conditions—even higher for diesel engines. Thus, adjusting ring tension to avoid ring collapse is unreasonable. [5] Ring tension is only useful for initially setting piston rings in a position where combustion gases can easily create the support forces behind the ring (to avoid ring collapse).

The equation governing whether ring collapse will occur is

$$\frac{(P_N + P_{N+1})A_{pouterface}}{2} > F_{tension} + P_{groove}A_{pinnerface} \quad (36)$$

where P_N is the pressure above ring N , P_{N+1} is the pressure below ring N ,

$A_{pouterface}$ is the projected ring face surface area in the radial direction, $F_{tension}$ is the

force due to ring tension, P_{groove} is the pressure in the groove behind the piston ring, and $A_{pinnerface}$ is the projected inner ring surface area in the radial direction.

When a piston ring collapses, a large area is opened up between the ring face and the cylinder liner. In order to find this area, the radial displacement of the piston ring must be defined. The radial displacement at any point of a ring is given by

$$\delta_r(\theta) = \frac{PR^4}{EI} \left(1 - \cos \theta + \frac{\theta}{2} \sin \theta \right) \quad (37)$$

where θ is the angular location of a point on a ring, P is the net radial load due to pressure and ring tension, R is the central radius of the ring, E is the modulus of elasticity of the ring material, and I is the moment of inertia of the ring cross section. Zero radians for θ is located on the side of the ring opposite of the ring gap.

The additional gas flow path that opens up in the event of ring collapse can then be defined as

$$A = 2 \int_0^\pi \delta_r R d\theta \quad (38)$$

Substituting Equation (37) into Equation (38), and solving the integral yields

$$A = \frac{3\pi PR^5}{EI} \quad (39)$$

the area added to the ring gap area in the gas flow calculations.

Under the circumstance that the ring end gap clearance is small, it is possible that the radial displacement may be restricted due to the ends of the ring butting. To find the maximum flow area that can occur between the ring face and the cylinder liner,

consider the area occupied by the piston ring, if its end clearance is zero. Before finding the area, the effective ring perimeter, p_{eff} must be calculated using

$$p_{eff} = \pi D - x_{endgap} \quad (40)$$

where D is the bore diameter (the original diameter of the outer ring surface) and x_{endgap} is the end gap clearance. An effective ring outer diameter D_{eff} can be found from Equation (40); it is defined as

$$D_{eff} = D - \frac{x_{endgap}}{\pi} \quad (41)$$

The area occupied by the ring, A_{ring} is simply

$$A_{ring} = \pi \frac{(D_{eff})^2}{4} \quad (42)$$

The maximum flow area, A_{max} , is by definition to be

$$A_{max} = A_{bore} - A_{ring} \quad (43)$$

where

$$A_{bore} = \frac{\pi D^2}{4} \quad (44)$$

So Equation (43) can be simplified in terms of end gap clearance and bore diameter such that

$$A_{max} = \frac{1}{2} x_{endgap} D \quad (45)$$

CHAPTER 4. COMPUTER SIMULATION VALIDATION

4.1 Overview

The CASE system has had much “real-world” testing and analysis. The uncalibrated past results in the correlate well with measured values. This chapter will provide a brief overview of how the CASE system results have compared to measured results in a past study on the same Ford 5.4 L engine. The Ford 5.4 L measured engine data was the only data set in which publishing permissions were given.

4.2 Comparisons

Figure 5 shows the measured blowby map values and Figure 6 shows the predicted blowby map values.

4.2.1 Comparing Predicted Blowby Maps

Figure 6's values appears to be different from the predicted values found in Figure 79. The difference applies to the interpretation of blowby. Ejakov's [6] definition of blowby was the amount of air flowing from the combustion chamber past the first compression ring. In this thesis, his definition is referred to as foreflow. This thesis defines blowby as the combination of foreflow and backflow. Therefore, if Ejakov's backflow results were summed with his blowby results, the end product would be identical to those found in Figure 79.

4.2.2 Comparing Measured and Predicted Blowby Maps

Figure 5 and Figure 6 show good overall trend correlation. The shape of the blowby map was slightly off in the high engine speed and low engine load region. However, the significant phenomenon of ring collapse was predicted by CASE in this

region. While the magnitude of the two plots differed slightly, their similarity was accurate enough such that valid predictions could be made from the CASE system results.

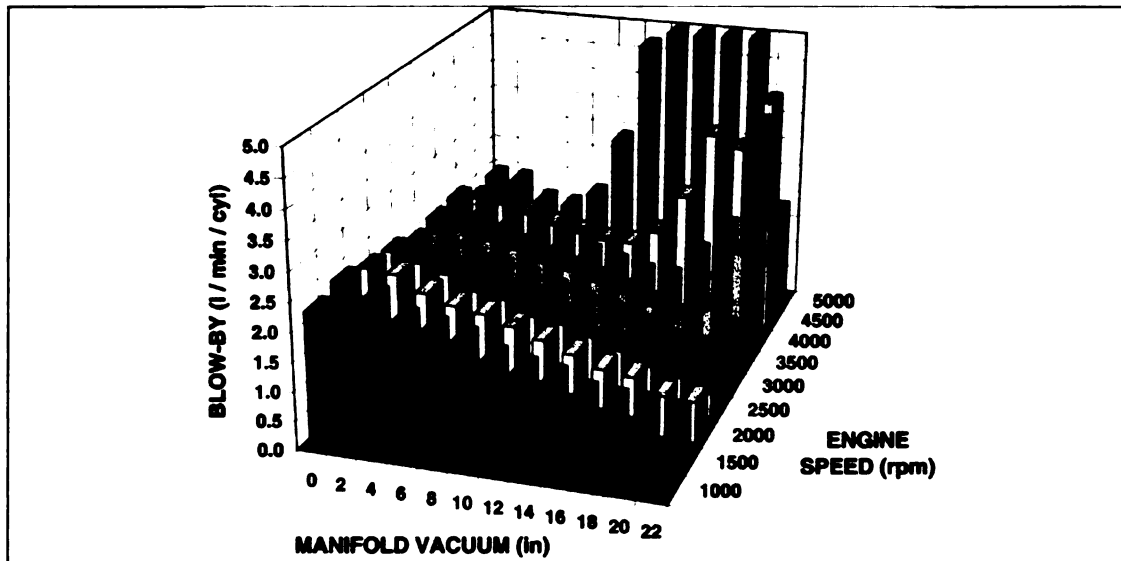


Figure 5: Ford 5.4 L V8 Engine Blowby Map - Measured [6]

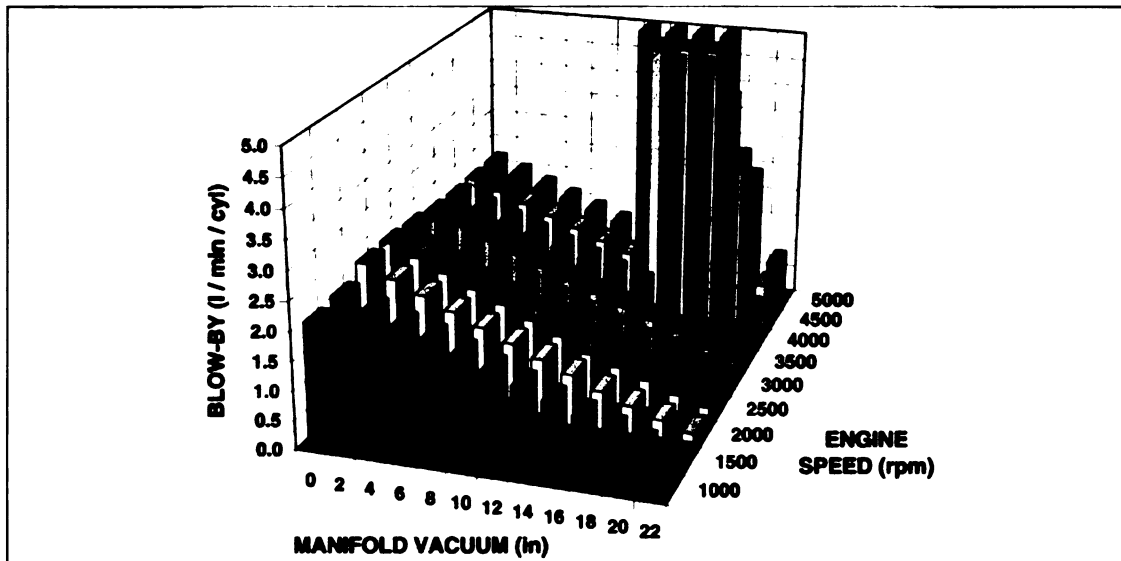


Figure 6: Ford 5.4 L V8 Engine Blowby Map - Predicted [6]

CHAPTER 5. COMPUTER SIMULATION SETUP

5.1 Simulation Hardware and Software

The cylinder kit simulation was performed using a computer of the following configuration:

Table 1: Computer Hardware

CPU	Intel Pentium III - 500 MHz
Motherboard	ABit BH6 - 100 MHz Bus
Memory	128 MB
Hard Disk	IBM EIDE 7200 RPM - 10 GB

The software used in the study is shown in Table 2.

Table 2: Computer Software

Operating System	Linux - Mandrake Distribution 7.0
Modeling Program	Cylinder kit Analysis System for Engines (CASE)
CASE Modules	RING, WebCASE
Web Server	Roxen Challenger 1.3

To expedite the parametric study on cylinder kit performance, a web page interface was created. The backend of the web page (CGI scripts) automatically calculated ring mass based on material density, and geometry of the piston ring. The crevice volumes described in Heading 2.2 were also automatically calculated using dimensions of the bore, piston and piston ring. Most importantly, WebCASE was developed to automate the

simulation of all operating conditions for any given cylinder kit configuration. Figure 7 summarizes the simulation process.

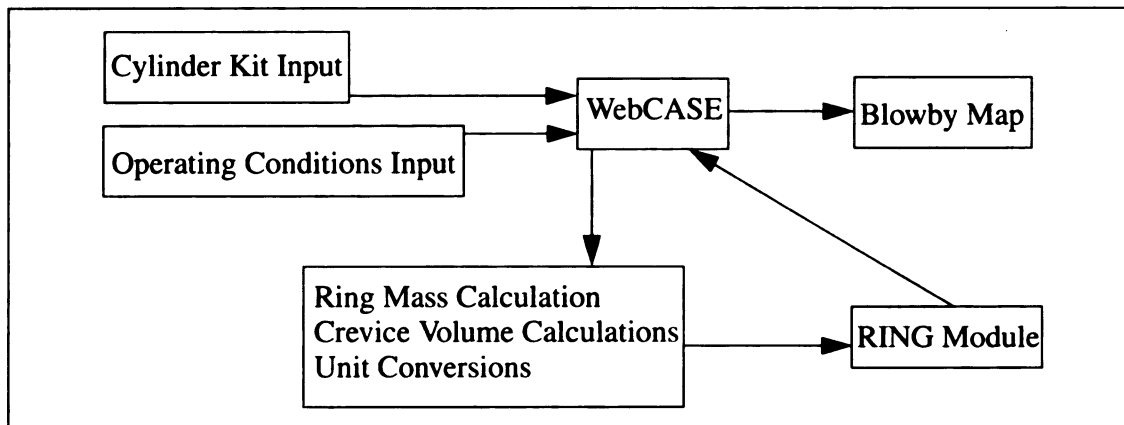


Figure 7: Process Flow Chart

5.2 Operating Conditions

The performance of ring packs varies greatly depending on operating conditions. Automobile engines must be designed to function for a large variety of operating conditions. Thus, the simulation was performed for 117 operating conditions for each geometry. Engine loads ranged from idling (0%) to maximum engine load (100%) in ~8.333% increments, and from 1000 to 5000 RPM in 500 RPM increments.

5.3 Cylinder Kit Schematics

This section contains simple schematics of cylinder kit components to help visualize dimensions and terminology described later in this thesis.

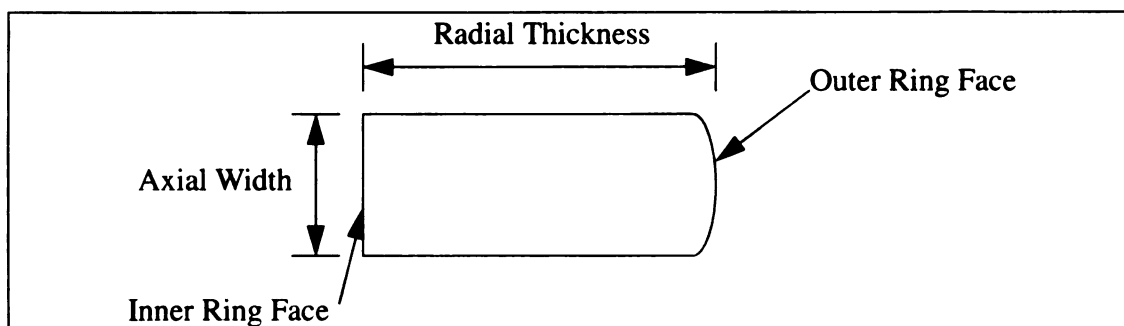


Figure 8: Piston Ring Cross Section

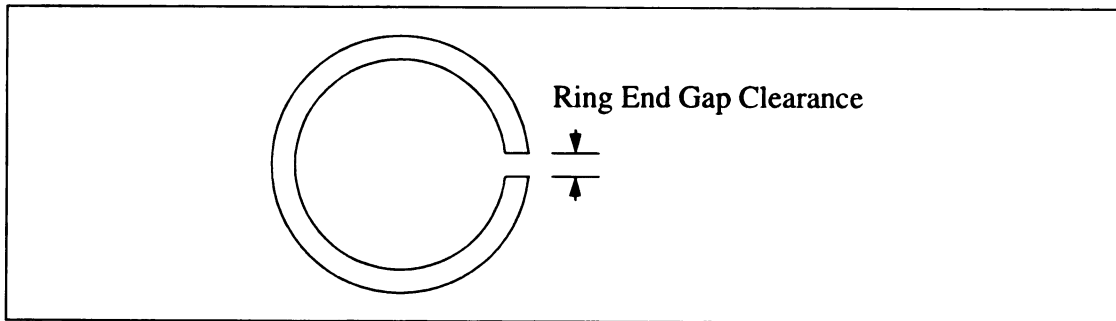


Figure 9: Piston Ring Top View

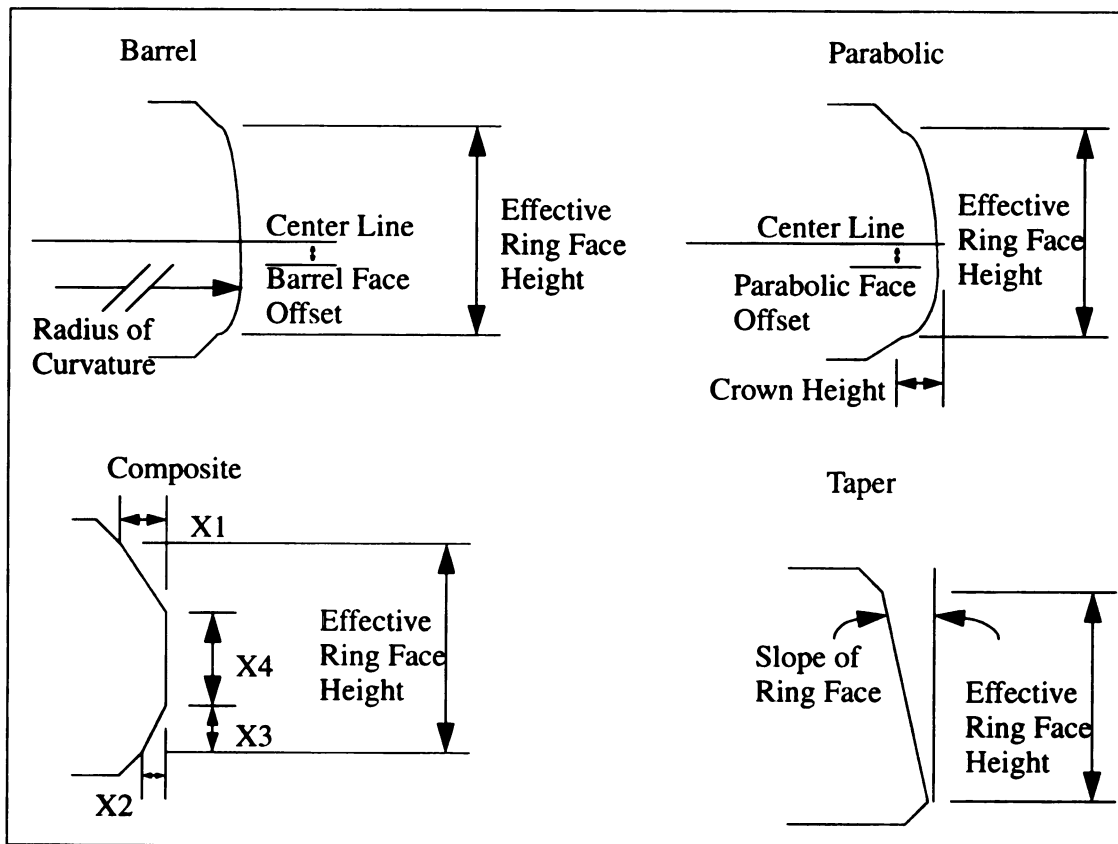


Figure 10: Piston Ring Face Profiles

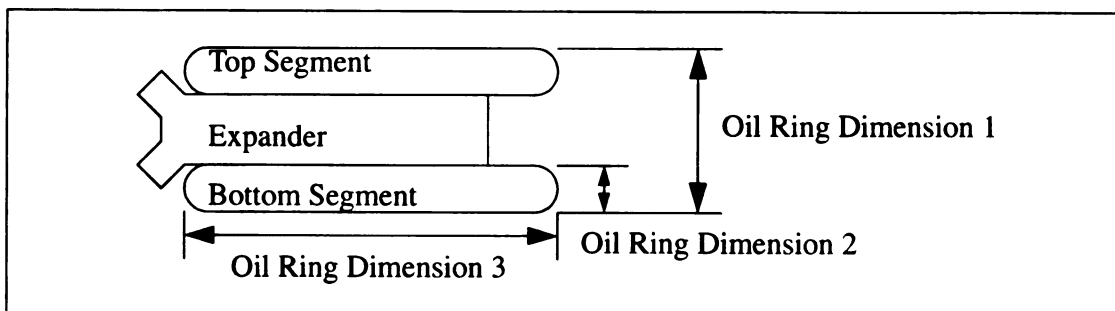


Figure 11: Three Piece Oil Ring Dimensions

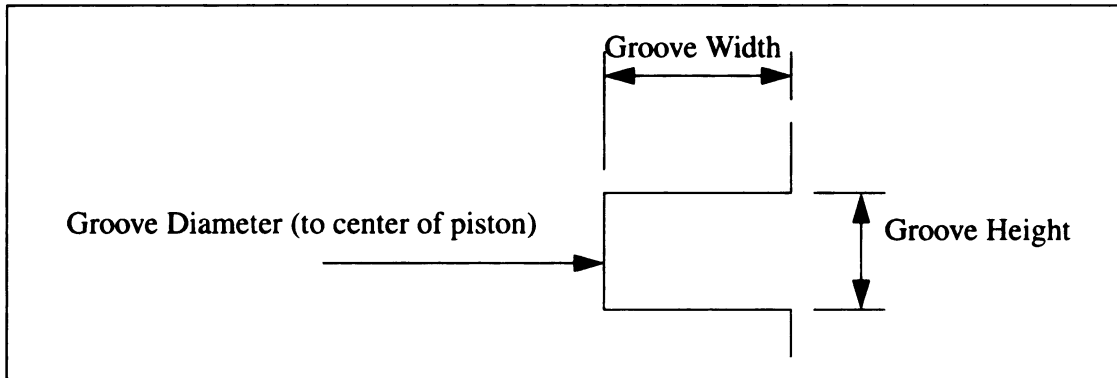


Figure 12: Piston Groove Cross Section

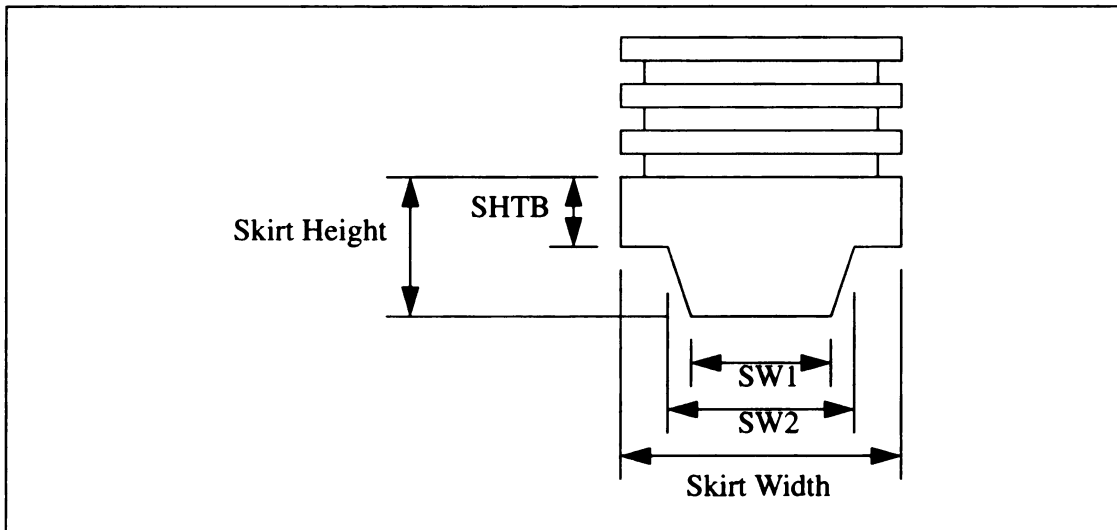


Figure 13: Skirt Dimensions

5.4 Engines Simulated

Three different Ford Motor Company engines were used in the parametric study performed for this thesis. These engines were a 5.4 L V8 engine, a 4.6 L V8 engine, and a 2.3 L I4 engine. All of these engines had similar original ring pack designs; the bore diameters of the engines were similar. The 5.4 L engine has the longest stroke, while the 2.3 L engine has the shortest stroke of the three engines. The exact cylinder kit specifications are as shown in Table 3, Table 4, and Table 5.

Table 3: Ford 5.4 L V8 2 Valve Cylinder Kit Specifications

Ring 1 = Top Compression Ring

Ring 2 = Second Compression Ring

Rings 4 and 5 = Oil Control Ring Segments

Parameter	Ring #	Value	Units
Number of Compression Rings		2	
Number of Oil Rings		1	
Piston Groove Height	1	1.53	mm
Piston Groove Width	1	3.5	mm
Piston Groove Diameter	1	82.2	mm
Ring Face Profile Type	1	parabolic	
Effective Ring Face Height	1	1.2	mm
Crown Height of Ring Face	1	0.009	mm
Ring Tension	1	23.8	N
Ring Mass	1	0.00965479	kg
Ring Modulus of Elasticity	1	9.6781E+10	Pa
Ring Poisson's Ratio	1	0.31	
Ring Mass Density	1	7196.8	kg/m ³
Ring Conduction Coefficient	1	63.0	W/(m*K)
Ring Coefficient of Thermal Expansion	1	6.55E-06	1/K
Axial Width (Ring Thickness)	1	1.45	mm
Radial Thickness (Ring Width)	1	3.4	mm
Ring Surface Roughness	1	0.000127	mm
Piston Groove Height	2	1.54	mm
Piston Groove Width	2	4.5	mm
Piston Groove Diameter	2	80.2	mm
Ring Face Profile Type	2	taper	
Effective Ring Face Height	2	1.45	mm
Ring Slope of Taper Face	2	2.0	deg
Ring Tension	2	28.9	N

Table 3: Ford 5.4 L V8 2 Valve Cylinder Kit Specifications

Ring 1 = Top Compression Ring

Ring 2 = Second Compression Ring

Rings 4 and 5 = Oil Control Ring Segments

Parameter	Ring #	Value	Units
Ring Mass	2	0.0110108	kg
Ring Modulus of Elasticity	2	8.9431E+10	Pa
Ring Poisson's Ratio	2	0.31	
Ring Mass Density	2	7196.8	kg/m ³
Ring Conduction Coefficient	2	63.0	W/(m*K)
Ring Coefficient of Thermal Expansion	2	6.55E-06	1/K
Ring Axial Width (Ring Thickness)	2	1.45	mm
Radial Thickness (Ring Width)	2	3.9	mm
Ring Surface Roughness	2	0.000127	mm
Piston Groove Height	4, 5	3.035	mm
Piston Groove Width	4, 5	4.15	mm
Piston Groove Diameter	4, 5	80.9	mm
Oil Ring Type	4, 5	Three-Piece	
Oil Control Ring Dimension 1	4, 5	3.015	mm
Oil Control Ring Dimension 2	4, 5	2.73	mm
Oil Control Ring Dimension 3	4, 5	0.478	mm
Ring Face Profile Type	4	barrel	
Effective Ring Face Height	4	0.478	mm
Radius of Curvature of Barrel Face	4	0.275	mm
Barrel Face Offset	4	0.0	mm
Ring Face Profile Type	5	barrel	
Effective Ring Face Height	5	0.478	mm
Radius of Curvature of Barrel Face	5	0.275	mm
Barrel Face Offset	5	0.0	mm
Ring Tension	4, 5	82.9	N

Table 3: Ford 5.4 L V8 2 Valve Cylinder Kit Specifications

Ring 1 = Top Compression Ring

Ring 2 = Second Compression Ring

Rings 4 and 5 = Oil Control Ring Segments

Parameter	Ring #	Value	Units
Ring Mass	4	0.0091	kg
Ring Modulus of Elasticity	4	2.068E+11	Pa
Ring Poisson's Ratio	4	0.3	
Ring Mass Density	4	7833.5	kg/m ³
Ring Conduction Coefficient	4	54.0	W/(m*K)
Ring Coefficient of Thermal Expansion	4	6.33E-06	1/K
Ring Modulus of Elasticity	5	2.068E+11	Pa
Ring Poisson's Ratio	5	0.3	
Ring Mass Density	5	7833.5	kg/m ³
Ring Conduction Coefficient	5	54.0	W/(m*K)
Ring Coefficient of Thermal Expansion	5	6.33E-06	1/K
Ring Surface Roughness	4, 5	0.000127	mm
End Gap Clearance	1	0.205	mm
End Gap Clearance	2	0.205	mm
End Gap Clearance	4	0.4	mm
Distance from Top of Piston to Compression Ring	1	6.27	mm
Distance from Top of Piston to Compression Ring	2	12.0050	mm
Distance from Top of Piston to Oil Control Ring	4, 5	16.99	mm
Crevice Volume Behind Compression Ring	1	241.8	mm ³
Land Crevice Volume Below Compression Ring	1	600.709	mm ³
Crevice Volume Behind Compression Ring	2	435.657	mm ³

Table 3: Ford 5.4 L V8 2 Valve Cylinder Kit Specifications

Ring 1 = Top Compression Ring

Ring 2 = Second Compression Ring

Rings 4 and 5 = Oil Control Ring Segments

Parameter	Ring #	Value	Units
Land Crevice Volume Below Compression Ring	2	385.812	mm ³
Volume Behind Oil Control Ring	4, 5	1522.22	mm ³
Connecting Rod Length		169.1	mm
Distance from Center of Crank Pin to Connecting Rod Center of Gravity		0.6582	mm
Connecting Rod Mass		0.6582	kg
Mass Moment of Inertia of Connecting Rod About Connecting Rod Center of Gravity		90.215	kg*m ²
Nominal Bore Diameter		90.215	mm
Piston Stroke		105.801	mm
Offset of Crank from Bore Center Line		0.0	mm
Distance from Top of Deck to Top of Piston When Piston Is at Top-Dead-Center (TDC)		3.0023	mm
Mass of Piston and Rings		0.359	kg
Mass Moment of Inertia of Piston About Piston Center of Gravity		3.8628E-06	kg*m ²
Piston Skirt Ovality		0.675	mm
Distance from Bottom of Cylinder to Bottom of Piston Skirt at Bottom-Dead-Center		6.50418	mm
Piston Pin Diameter		22.0	mm
Pin Offset in X-Direction		-1.0	mm
Pin Offset in Y-Direction		31.0	mm
Piston Diameter		89.2	mm
Piston Height		52.0	mm

Table 3: Ford 5.4 L V8 2 Valve Cylinder Kit Specifications

Ring 1 = Top Compression Ring

Ring 2 = Second Compression Ring

Rings 4 and 5 = Oil Control Ring Segments

Parameter	Ring #	Value	Units
X-Coordinate of Piston Center of Gravity		-0.000999	mm
Y-Coordinate of Piston Center of Gravity		-0.005	mm
Thickness of Pin Boss		21.575	mm
Thickness of Crown		8.0	mm
Piston Modulus of Elasticity		7.9979E+10	Pa
Piston Poisson's Ratio		0.33	
Piston Mass Density		2698.8	kg/m ³
Piston Conduction Coefficient		161.0	W/(m*K)
Piston Coefficient of Thermal Expansion		1.03E-05	1/K
Mean Combustion Chamber Temperature		478.0	C
Mean Sump Temperature		336.0	C
Mean Temperature Behind Compression Ring	1	433.0	C
Mean Land Temperature Below Compression Ring	1	428.0	C
Mean Temperature Behind Compression Ring	2	422.0	C
Mean Land Temperature Below Compression Ring	2	411.0	C
Temperature Behind Oil Control Ring	4, 5	400.0	C
Skirt Height		33.5	mm
Skirt Width		70.0	mm
Skirt Dimension (SHTB)		0.0	mm
Skirt Dimension (SW1)		0.0	mm

Table 3: Ford 5.4 L V8 2 Valve Cylinder Kit Specifications

Ring 1 = Top Compression Ring

Ring 2 = Second Compression Ring

Rings 4 and 5 = Oil Control Ring Segments

Parameter	Ring #	Value	Units
Skirt Dimension (SW2)		0.0	mm
SAE Oil Type		30	

Table 4: Ford 4.6 L V8 2 Valve Cylinder Kit Specifications

Ring 1 = Top Compression Ring

Ring 2 = Second Compression Ring

Rings 4 and 5 = Oil Control Ring Segments

Parameter	Ring #	Value	Units
Number of Compression Rings		2	
Number of Oil Rings		1	
Piston Groove Height	1	1.524	mm
Piston Groove Width	1	4.5	mm
Piston Groove Diameter	1	80.71	mm
Ring Face Profile Type	1	barrel	
Effective Ring Face Height	1	1.22	mm
Radius of Curvature of Barrel Face	1	13.0	mm
Ring Tension	1	25.35	N
Ring Mass	1	0.0112101	kg
Ring Modulus of Elasticity	1	9.67810E+10	Pa
Ring Poisson's Ratio	1	0.31	
Ring Mass Density	1	7196.8	kg/m ³
Ring Conduction Coefficient	1	63.0	W/(m*K)
Ring Coefficient of Thermal Expansion	1	6.55E-06	1/K
Axial Width (Ring Thickness)	1	1.47	mm
Radial Thickness (Ring Width)	1	3.965	mm
Ring Surface Roughness	1	5.1E-05	mm

Table 4: Ford 4.6 L V8 2 Valve Cylinder Kit Specifications
Ring 1 = Top Compression Ring
Ring 2 = Second Compression Ring
Rings 4 and 5 = Oil Control Ring Segments

Parameter	Ring #	Value	Units
Piston Groove Height	2	1.524	mm
Piston Groove Width	2	4.61	mm
Piston Groove Diameter	2	80.48	mm
Ring Face Profile Type	2	taper	
Effective Ring Face Height	2	0.923	mm
Ring Slope of Taper Face	2	1.76	deg
Ring Tension	2	27.58	N
Ring Mass	2	0.0116641	kg
Ring Modulus of Elasticity	2	8.94310E+10	Pa
Ring Poisson's Ratio	2	0.31	
Ring Mass Density	2	7196.80	kg/m ³
Ring Conduction Coefficient	2	63.0	W/(m*K)
Ring Coefficient of Thermal Expansion	2	6.55000E-06	1/K
Ring Axial Width (Ring Thickness)	2	1.479	mm
Radial Thickness (Ring Width)	2	4.07	mm
Ring Surface Roughness	2	5.1E-05	mm
Piston Groove Height	4, 5	3.02	mm
Piston Groove Width	4, 5	3.508	mm
Piston Groove Diameter	4, 5	82.68	mm
Oil Ring Type	4, 5	Three-Piece	
Oil Control Ring Dimension 1	4, 5	2.92	mm
Oil Control Ring Dimension 2	4, 5	2.69	mm
Oil Control Ring Dimension 3	4, 5	0.46	mm
Ring Face Profile Type	4	barrel	
Effective Ring Face Height	4	1.0	mm

Table 4: Ford 4.6 L V8 2 Valve Cylinder Kit Specifications

Ring 1 = Top Compression Ring

Ring 2 = Second Compression Ring

Rings 4 and 5 = Oil Control Ring Segments

Parameter	Ring #	Value	Units
Radius of Curvature of Barrel Face	4	1.0	mm
Barrel Face Offset	4	0.229	mm
Ring Face Profile Type	5		
Effective Ring Face Height	5	0.41	mm
Radius of Curvature of Barrel Face	5	1.0	mm
Barrel Face Offset	5	0.229	mm
Ring Tension	4, 5	82.9	N
Ring Mass	4	0.0091	kg
Ring Modulus of Elasticity	4	2.068E+11	Pa
Ring Poisson's Ratio	4	0.3	
Ring Mass Density	4	7833.5	kg/m ³
Ring Conduction Coefficient	4	54.0	W/(m*K)
Ring Coefficient of Thermal Expansion	4	6.33E-06	1/K
Ring Modulus of Elasticity	5	2.068E+11	Pa
Ring Poisson's Ratio	5	0.3	
Ring Mass Density	5	7833.5	kg/m ³
Ring Conduction Coefficient	5	54.0	W/(m*K)
Ring Coefficient of Thermal Expansion	5	6.33E-06	1/K
Ring Surface Roughness	4, 5	5.1E-05	mm
End Gap Clearance	1	0.3556	mm
End Gap Clearance	2	0.4445	mm
End Gap Clearance	4	0.3429	mm
Distance from Top of Piston to Compression Ring	1	6.37	mm

Table 4: Ford 4.6 L V8 2 Valve Cylinder Kit Specifications
Ring 1 = Top Compression Ring
Ring 2 = Second Compression Ring
Rings 4 and 5 = Oil Control Ring Segments

Parameter	Ring #	Value	Units
Distance from Top of Piston to Compression Ring	2	11.71	mm
Distance from Top of Piston to Oil Control Ring	4, 5	16.5	mm
Crevice Volume Behind Compression Ring	1	833.955	mm ³
Land Crevice Volume Below Compression Ring	1	263.129	mm ³
Crevice Volume Behind Compression Ring	2	306.999	mm ³
Land Crevice Volume Below Compression Ring	2	177.174	mm ³
Volume Behind Oil Control Ring	4, 5	849.404	mm ³
Connecting Rod Length		150.7	mm
Distance from Center of Crank Pin to Connecting Rod Center of Gravity		50.2	mm
Connecting Rod Mass		1.109	kg
Mass Moment of Inertia of Connecting Rod About Connecting Rod Center of Gravity		1.99E-06	kg*m ²
Nominal Bore Diameter		90.198	mm
Piston Stroke		90.0	mm
Offset of Crank from Bore Center Line		0.0	mm
Distance from Top of Deck to Top of Piston When Piston Is at Top-Dead-Center (TDC)		1.82	mm
Mass of Piston and Rings		0.1078	kg
Mass Moment of Inertia of Piston About Piston Center of Gravity		0.000877	kg*m ²

Table 4: Ford 4.6 L V8 2 Valve Cylinder Kit Specifications

Ring 1 = Top Compression Ring

Ring 2 = Second Compression Ring

Rings 4 and 5 = Oil Control Ring Segments

Parameter	Ring #	Value	Units
Piston Skirt Ovality		0.508	mm
Distance from Bottom of Cylinder to Bottom of Piston Skirt at Bottom-Dead-Center		0.0	mm
Piston Pin Diameter		22.0	mm
Pin Offset in X-Direction		-1.27	mm
Pin Offset in Y-Direction		31.0	mm
Piston Diameter		89.71	mm
Piston Height		56.39	mm
X-Coordinate of Piston Center of Gravity		-0.999	mm
Y-Coordinate of Piston Center of Gravity		-5.0	mm
Thickness of Pin Boss		5.0	mm
Thickness of Crown		6.955	mm
Piston Modulus of Elasticity		7.9979E+10	Pa
Piston Poisson's Ratio		0.33	
Piston Mass Density		2698.8	kg/m ³
Piston Conduction Coefficient		161.0	W/(m*K)
Piston Coefficient of Thermal Expansion		1.03E-05	1/K
Mean Combustion Chamber Temperature		204.85	C
Mean Sump Temperature		92.85	C
Mean Temperature Behind Compression Ring	1	159.85	C
Mean Land Temperature Below Compression Ring	1	154.85	C

Table 4: Ford 4.6 L V8 2 Valve Cylinder Kit Specifications

Ring 1 = Top Compression Ring

Ring 2 = Second Compression Ring

Rings 4 and 5 = Oil Control Ring Segments

Parameter	Ring #	Value	Units
Mean Temperature Behind Compression Ring	2	148.85	C
Mean Land Temperature Below Compression Ring	2	137.85	C
Temperature Behind Oil Control Ring	4, 5	126.85	C
Skirt Height		38.4	mm
Skirt Width		69.6	mm
Skirt Dimension (SHTB)		0.0	mm
Skirt Dimension (SW1)		0.0	mm
Skirt Dimension (SW2)		0.0	mm
SAE Oil Type		30	

Table 5: Ford 2.3 L I4 2 Valve Cylinder Kit Specifications

Ring 1 = Top Compression Ring

Ring 2 = Second Compression Ring

Rings 4 and 5 = Oil Control Ring Segments

Parameter	Ring #	Value	Units
Number of Compression Rings		2	
Number of Oil Rings		1	
Piston Groove Height	1	1.5301	mm
Piston Groove Width	1	4.49301	mm
Piston Groove Diameter	1	86.9932	mm
Ring Face Profile Type	1	parabolic	
Effective Ring Face Height	1	1.47648	mm
Crown Height of Ring Face	1	0.228600	mm
Ring Tension	1	21.75	N
Ring Mass	1	0.0120999	kg

Table 5: Ford 2.3 L I4 2 Valve Cylinder Kit Specifications

Ring 1 = Top Compression Ring

Ring 2 = Second Compression Ring

Rings 4 and 5 = Oil Control Ring Segments

Parameter	Ring #	Value	Units
Ring Modulus of Elasticity	1	9.67808E+10	Pa
Ring Poisson's Ratio	1	0.31	
Ring Mass Density	1	7196.79	kg/m ³
Ring Conduction Coefficient	1	63.0	W/(m*K)
Ring Coefficient of Thermal Expansion	1	6.55E-05	1/K
Axial Width (Ring Thickness)	1	1.47648	mm
Radial Thickness (Ring Width)	1	3.94971	mm
Ring Surface Roughness	1	0.000127	mm
Piston Groove Height	2	1.5301	mm
Piston Groove Width	2	4.49301	mm
Piston Groove Diameter	2	86.9932	mm
Ring Face Profile Type	2	taper	
Effective Ring Face Height	2	1.07442	mm
Ring Slope of Taper Face	2	0.75	deg
Ring Tension	2	20.2998	N
Ring Mass	2	0.0122343	kg
Ring Modulus of Elasticity	2	8.94307E+10	Pa
Ring Poisson's Ratio	2	0.31	
Ring Mass Density	2	7196.79	kg/m ³
Ring Conduction Coefficient	2	63.0	W/(m*K)
Ring Coefficient of Thermal Expansion	2	6.55E-06	1/K
Ring Axial Width (Ring Thickness)	2	1.47648	mm
Radial Thickness (Ring Width)	2	4.0	mm
Ring Surface Roughness	2	0.000127	mm
Piston Groove Height	4, 5	3.04039	mm

Table 5: Ford 2.3 L I4 2 Valve Cylinder Kit Specifications

Ring 1 = Top Compression Ring

Ring 2 = Second Compression Ring

Rings 4 and 5 = Oil Control Ring Segments

Parameter	Ring #	Value	Units
Piston Groove Width	4, 5	3.50521	mm
Piston Groove Diameter	4, 5	88.9688	mm
Oil Ring Type	4, 5	Three-Piece	
Oil Control Ring Dimension 1	4, 5	2.91059	mm
Oil Control Ring Dimension 2	4, 5	2.48920	mm
Oil Control Ring Dimension 3	4, 5	0.407417	mm
Ring Face Profile Type	4	Composite	
Effective Ring Face Height	4	0.406401	mm
Ring Face Parameter X1	4	0.0508001	mm
Ring Face Parameter X2	4	0.0508001	mm
Ring Face Parameter X3	4	0.0830582	mm
Ring Face Parameter X4	4	0.24892	mm
Ring Face Profile Type	5	Composite	
Effective Ring Face Height	5	0.406401	mm
Ring Face Parameter X1	5	0.0508001	mm
Ring Face Parameter X2	5	0.0508001	mm
Ring Face Parameter X3	5	0.0830582	mm
Ring Face Parameter X4	5	0.24892	mm
Ring Tension	4, 5	70.0178	N
Ring Mass	4	0.00798331	kg
Ring Modulus of Elasticity	4	2.06800E+11	Pa
Ring Poisson's Ratio	4	0.3	
Ring Mass Density	4	7833.49	kg/m ³
Ring Conduction Coefficient	4	54.0	W/(m*K)
Ring Coefficient of Thermal Expansion	4	6.33E-06	1/K

Table 5: Ford 2.3 L I4 2 Valve Cylinder Kit Specifications

Ring 1 = Top Compression Ring

Ring 2 = Second Compression Ring

Rings 4 and 5 = Oil Control Ring Segments

Parameter	Ring #	Value	Units
Ring Modulus of Elasticity	5	2.06800E+11	Pa
Ring Poisson's Ratio	5	0.3	
Ring Mass Density	5	7833.49	kg/m ³
Ring Conduction Coefficient	5	54.0	W/(m*K)
Ring Coefficient of Thermal Expansion	5	6.33E-06	1/K
Ring Surface Roughness	4, 5	0.000127	mm
End Gap Clearance	1	0.304801	mm
End Gap Clearance	2	0.406401	mm
End Gap Clearance	4	0.505461	mm
Distance from Top of Piston to Compression Ring	1	7.03073	mm
Distance from Top of Piston to Compression Ring	2	12.3749	mm
Distance from Top of Piston to Oil Control Ring	4, 5	17.2085	mm
Crevice Volume Behind Compression Ring	1	235.595	mm ³
Land Crevice Volume Below Compression Ring	1	18.9675	mm ³
Crevice Volume Behind Compression Ring	2	214.306	mm ³
Land Crevice Volume Below Compression Ring	2	12.6731	mm ³
Volume Behind Oil Control Ring	4, 5	887.601	mm ³
Connecting Rod Length		138.621	mm
Distance from Center of Crank Pin to Connecting Rod Center of Gravity		57.1501	mm
Connecting Rod Mass		0.649097	kg

Table 5: Ford 2.3 L I4 2 Valve Cylinder Kit Specifications

Ring 1 = Top Compression Ring

Ring 2 = Second Compression Ring

Rings 4 and 5 = Oil Control Ring Segments

Parameter	Ring #	Value	Units
Mass Moment of Inertia of Connecting Rod About Connecting Rod Center of Gravity		5.85258E-06	kg*m ²
Nominal Bore Diameter		96.0122	mm
Piston Stroke		79.4006	mm
Offset of Crank from Bore Center Line		0.0	mm
Distance from Top of Deck to Top of Piston When Piston Is at Top-Dead-Center (TDC)		4.06401	mm
Mass of Piston and Rings		0.130182	kg
Mass Moment of Inertia of Piston About Piston Center of Gravity		1.0242E-06	kg*m ²
Piston Skirt Ovality		0.0	mm
Distance from Bottom of Cylinder to Bottom of Piston Skirt at Bottom-Dead-Center		11.778	mm
Piston Pin Diameter		23.1648	mm
Pin Offset in X-Direction		-1.524	mm
Pin Offset in Y-Direction		34.1910	mm
Piston Diameter		95.9792	mm
Piston Height		66.7005	mm
X-Coordinate of Piston Center of Gravity		1.524	mm
Y-Coordinate of Piston Center of Gravity		19.05	mm
Thickness of Pin Boss		5.00127	mm
Thickness of Crown		6.99771	mm
Piston Modulus of Elasticity		7.99793	Pa

Table 5: Ford 2.3 L I4 2 Valve Cylinder Kit Specifications

Ring 1 = Top Compression Ring

Ring 2 = Second Compression Ring

Rings 4 and 5 = Oil Control Ring Segments

Parameter	Ring #	Value	Units
Piston Poisson's Ratio		0.33	
Piston Mass Density		2698.8	kg/m ³
Piston Conduction Coefficient		161.0	W/(m*K)
Piston Coefficient of Thermal Expansion		1.03E-05	1/K
Mean Combustion Chamber Temperature		454.444	C
Mean Sump Temperature		93.8889	C
Mean Temperature Behind Compression Ring	1	203.889	C
Mean Land Temperature Below Compression Ring	1	176.111	C
Mean Temperature Behind Compression Ring	2	162.778	C
Mean Land Temperature Below Compression Ring	2	148.333	C
Temperature Behind Oil Control Ring	4, 5	135.0	C
Skirt Height		47.9553	mm
Skirt Width		70.9931	mm
Skirt Dimension (SHTB)		15.6972	mm
Skirt Dimension (SW1)		40.9449	mm
Skirt Dimension (SW2)		21.3614	mm
SAE Oil Type		SAE Grade 30	

5.5 Gas Pressure Input Data

The RING program of the Cylinder kit Analysis System for Engines requires in-cylinder combustion pressure over the entire engine cycle as an input; it is required to perform ring pack performance calculations. These in-cylinder combustion pressures for

this study were obtained from another simulation program called General Engine Simulation (GESIM).

The GESIM program, a part of Ford Motor Company's ENGINE SIMulation system (ENGsim), simulates in-cylinder flow (in the combustion chamber), heat transfer, and thermodynamics for both motoring and firing conditions. Pressure points were generated for engine speeds varying from 1000 to 5000 RPM in 500 RPM increments and engine loads from 0 (full load) to 558.8 mm (idling) of manifold vacuum with 50.8 mm increments for all engines.

5.6 Ring Geometry Input Data

5.6.1 Primary Parametric Study

The original piston ring geometry for each ring and engine is shown in Table 3, Table 4 and Table 5. Piston ring dimensions were altered to measure their influence on engine blowby performance. The test matrices are given in Table 6, Table 7 and Table 8.

Table 6: Ford 5.4 L V8 Engine Top Compression Ring Test Matrix

Parameter	Values
End Gap Clearance	0.3, 0.5, 0.7, 0.9
Axial Width	1.46, 1.47, 1.48, 1.49, 1.50, 1.51, 1.52
Radial Thickness	3.2, 3.3, 3.4, 3.5, 3.6, 3.7, 3.8, 3.9, 4.0

Table 7: Ford 4.6 L V8 Engine Top Compression Ring Test Matrix

Parameter	Values
End Gap Clearance	0.4, 0.5, 0.6, 0.7, 0.8, 0.9, 1.0, 1.1, 1.2, 1.3
Axial Width	1.48, 1.49, 1.50, 1.51, 1.52
Radial Thickness	4.1, 4.3, 4.5, 4.7

Table 8: Ford 2.3 L I4 Engine Top Compression Ring Test Matrix

Parameter	Values
End Gap Clearance	0.4, 0.5, 0.6, 0.7, 0.9
Axial Width	1.47, 1.48, 1.49, 1.50, 1.51, 1.52
Radial Thickness	4.0, 4.1, 4.2, 4.3, 4.4

In reading these tables, one notices that the parametric values vary from engine to engine. The same values often could not be selected in some instances due to geometric conflicts. That is, there are geometric constraints such as groove width, groove diameter, and bore diameter preventing certain geometries from being tested. The increments varied depending upon the rate at which blowby performance was affected.

Unfortunately due to the nature of this study, it was physically impossible to modify single parameters independently. The ring end gap clearance cannot be modified without also changing the ring mass and the flow area through gap. Ring tension and ring mass increase proportionally as axial width increases. Increasing radial thickness decreases the crevice volume behind the ring and increases ring mass. These by-product parameters made data analysis more challenging, but not impossible.

5.6.2 Secondary Parametric Study

A mini-study was performed to observe the effects (if any) that the second compression ring had on the overall gas sealing performance of the ring pack. The test matrix is given below.

Table 9: Ford 5.4 L V8 Engine Top and Second Compression Ring Test Matrix

Parameter	Values
End Gap Clearance	0.3, 0.4, 0.5, 0.6, 0.7, 0.8, 0.9

5.7 Bore, Piston, and Connecting Rod Data

Piston groove dimensions were altered to measure their influence on engine blowby performance. The test matrices are given in Table 10, Table 11 and Table 12.

Table 10: Ford 5.4 L V8 Engine Top Piston Groove Test Matrix

Parameter	Values
Groove Height	1.46, 1.47, 1.48, 1.49, 1.50, 1.51, 1.52, 1.54, 1.55
Groove Diameter	82.00, 82.40, 82.60, 82.80, 83.00, 83.20

Table 11: Ford 4.6 L V8 Engine Top Piston Groove Test Matrix

Parameter	Values
Groove Height	1.48, 1.49, 1.50, 1.51, 1.52
Groove Diameter	80.91, 81.11, 81.31, 81.51, 81.71, 81.91, 82.11, 82.20

Table 12: Ford 2.3 L V8 Engine Top Piston Groove Test Matrix

Parameter	Values
Groove Height	1.49, 1.50, 1.51, 1.52, 1.54
Groove Diameter	87.10, 87.30, 87.50, 87.70, 87.90

The groove dimensions, like the ring dimensions, also had “by-product” parameters. An increase in groove height resulted in an increase in crevice volume. As the groove diameter was increased, the crevice volume decreased. Additionally, groove width had to decrease as groove diameter increased, so that piston diameter would not have to increase. Thus, the groove became shallower, as groove diameter was increased. Neglecting these by-product parameters would make analysis of the results nonsensical.

5.8 Ring Twist

In real engines, the piston rings with non-symmetric cross sections “twist” in their groove throughout the engine cycle. Thus, the ring not only moves axially, but

different sections of the rings twist and occupy different axial locations at the same instance of time. The phenomenon of ring twist affects gas flow areas and ring wear patterns. Although the TWIST program in the Cylinder kit Analysis System for Engines, supports ring twist simulation, it was not utilized in this study due to technical complications.

In order for ring twist to be accounted for in the simulations several issues would have to be resolved. The most challenging of these issues would be to develop an automated finite element gridding program. Piston rings vary greatly in size and shape, thus making it difficult to code an algorithm to produce an evenly-sized grid, utilizing quadrilaterals and triangles of proper aspect ratio (elements that are not extremely narrow or skewed). The second technical issue was the large amount of computer cycles that would be required to generate stiffness matrices from the finite element grid, and 3-D ring positions from the force vectors. With a Pentium III 500 MHz processor, it takes between three to seven hours (depending upon the presence of ring collapse) to compute fully ring pack performance with twist for one operating point. The ring twist analysis would have to be done separately for each of the 117 operating conditions multiplied by the several cylinder kit designs; it may have taken up to one year of computer time to calculate the data points for this study. However, in the near future, computing technology may make the full ring twist analysis for the entire engine operating maps economically and temporally feasible.

Due to the circumstances explained above, ring twist was omitted from this study. Fortunately, the piston ring cross sections for this study were almost perfectly

rectangular and symmetric (radially and axially), meaning that the extent of ring twist presence in these cases are not a strong influence even in the real engine.

CHAPTER 6. COMPUTER SIMULATION RESULTS

6.1 Overview

In all instances, the Ford 4.6 L V8 engine had the worst blowby performance of the three engines. The Ford 5.4 L V8 engine had the most unstable ring pack; that is, it collapsed the most often. The Ford 2.3 L I4 engine had the most desirable blowby performance and stability.

6.2 Plots

Due to the large volume of relevant plots produced in this parametric study, the complete set of blowby map plots has been included in Appendix A (Chapter 10).

Images in this thesis are presented in color.

CHAPTER 7. COMPUTER SIMULATION ANALYSIS

7.1 Blowby Map Analysis

Blowby maps can provide useful information on the performance of piston ring packs for a range of operating conditions. By comparing multiple different blowby maps, one can observe the degree of influence certain parameters have on blowby performance.

In general, nominal engine performance is characterized by the following traits on blowby maps:

1. As engine speed increases, blowby increases.
2. Engine speed has more influence on blowby at higher engine loads.
3. As engine load increases, blowby increases.
4. Engine load has more influence on blowby than engine speed.
5. The blowby map forms an almost perfectly smooth plane.

Figure 14 illustrates the shape of a typical blowby map for an engine.

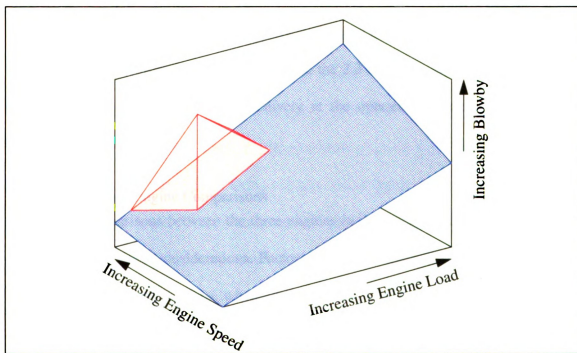


Figure 14: Typical Blowby Map

The crosshatched region in Figure 14 indicates area of "normal ring performance." The dotted region represents the area that is the most likely to have ring

collapse. Ring collapse in blowby maps is usually detected by a cone, or ridge protruding sharply from the plane. Minor bumps and ridges are usually signs of ring fluttering.

7.2 General Observations

7.2.1 Effect of Blowby Magnitude on Parameter Sensitivity

Typically, the greater the blowby at an operating condition, the greater the influence parameter variations had on the sealing performance. Therefore, the degree of impact of parameter variations can easily be gauged by observing the operating conditions of highest engine loads and engine speeds, and operating conditions attributed with ring collapse.

A comparison of the plots in Heading 10.2, Heading 10.3 and Heading 10.4 reveals the differing parameter sensitivity characteristics of the three engines studied. The 4.6 L engine had the overall highest blowby, and thus had the most parameter sensitivity. Since the overall blowby was relatively low in the 2.3 L engine, most of the parametric effects could only be observed qualitatively at the operating conditions with highest blowby.

7.2.2 Note on Engine Comparisons

Comparisons between the three engines in this study cannot be made directly without taking special considerations. Factors such as compression ratio and stroke can strongly affect the results. Thus, when comparing the engines, one should analyze their trends and not their magnitudes.

The 2.3 L cylinder kit appeared to have the best performance and stability of the three engines. However, the in-cylinder peak pressure was also significantly lower than that of the other engines. The 4.6 L cylinder kit's poor blowby performance was attributed

primarily to its high in-cylinder peak pressure. While theoretical thermodynamics dictates that higher compression ratios lead to higher engine efficiency, in practice, higher compression ratios sometimes lower sealing efficiencies.

The 5.4 L cylinder kit is interesting because its overall blowby performance and compression ratio lies between the two other engines, but its ring pack stability is also the worst. Its longer stroke contributes to inertial effects, bringing ring collapse into its operating conditions set. Changing stroke and compression ratio can move ring collapse inside or outside an engines operating conditions.

7.3 End Gap Analysis

Agreeing with Wentworth's [12] results, the plots in Heading 10.2.2, Heading 10.3.2 and Heading 10.4.2 show that blowby smoothly increased at all operating points for all the engines as the top ring end gap increased. This observation may at first seem obvious, because the flow area is being increased. However, if one also examines the inertial effects, this observation may no longer be trivial.

Coinciding with Equation (45), a reduction in ring gap caused a reduction in blowby in operating conditions with ring collapse. As explained in Heading 3.4, if the ring gap is sufficiently small, the two ends of the ring butt together during ring collapse, thereby preventing the ring from collapsing all the way.

As the ring gap is increased, the amount of ring material is decreased. Decreases in ring mass tend to improve ring pack sealing performance by reducing the likelihood of ring collapse (see Heading 3.4). In studying the plots in Heading 10.4.2, the number of operating conditions with ring collapse was shown to become worse when the

end gap was reduced. Thus, an unknown ring destabilizing factor was present. A mini-study was performed to discover this unknown influence.

7.3.1 Mini-Study on 5.4 L V8 Ford Motor Company Engine

The mini-study showed that the second ring sealing performance had a strong effect on the top ring sealing performance, under certain conditions. According to the plots in Heading 10.5, opening the end gap wider for the second compression ring did not significantly increase blowby for most operating conditions. However, widening the second ring end gap increased the piston ring stability; the number of operating points with ring collapse was higher when the top compression ring end gap was exclusively increased.

The cause of this behavior is related to the forces exerted on the top ring. Gas flows into the piston land below the top ring. Since the second ring end gap is smaller than that of the top ring, the gases are not allowed to flow past the second ring as easily. Thus, pressure increases in the volume between the top and second ring, which in turn generates a force upward on the top ring. This upward force combined with the inertial effects accelerates the piston ring toward the top of its groove. As explained in Heading 3.4, if the top piston ring arrives at the top of its groove late in the compression stroke, the conditions are likely to lead to ring collapse. Therefore, if ring collapse is problematic for a given ring pack, the second ring end gap can be increased to improve the ring pack's stability without severely degrading the ring pack performance.

One important aspect to note is that increasing the second ring end gap has an additional undesirable effect. Besides slightly increasing the blowby at each operating point, operating points with ring collapse had significantly higher blowby—as shown in

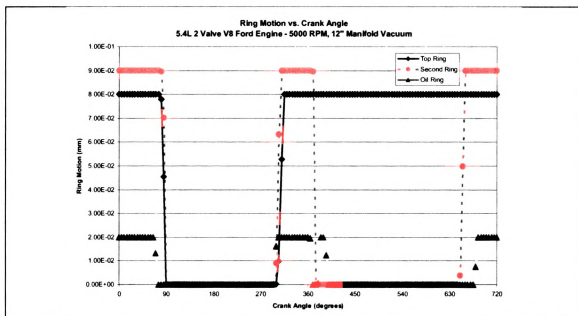


Figure 15: Ring Motion Versus Crank Angle (Ring Collapse)

Figure 86 and Figure 126. The blowby magnitudes in the case of ring collapse are higher because the larger second ring gap allows for an increased flow rate. In these instances, the second compression ring sometimes collapsed as the additional gas flowed through the second ring end gap. This flow accumulated pressure below the second ring. This pressure below the second ring can force the ring to the top of its groove near the end of compression. Thus, following a top ring collapse, the second ring may also collapse if the second ring gap is too large.

It is important to note that from this mini-study, one can see that anytime that the second ring seals better than the top ring, the force balance would tend to favor a ring collapse condition. Although it initially seems absurd to expand the ring gap (under certain conditions) to improve blowby performance, others such as Vaccino [13] and Federal Mogul [14] hypothesized similar explanations.

7.3.2 Note of Caution

Although reducing the end gap improves both general performance and performance during ring collapse, there exists a lower limit for the ring gap. If the ring gap is too small, thermal expansion can cause the ends of the ring to butt together and cause extreme ring and liner wear. All of the dimensions run in the simulations are assumed to be “warm” dimensions. Therefore, actual compression ring end gap designs would be larger than the “warm” dimensions.

7.4 Axial Width Analysis

Axial width for the top compression ring had only an almost negligible influence on blowby performance. Blowby decreased very slightly as the axial width of the piston ring was reduced. When the axial width of the ring approached 10 to 20 microns of its ring groove height, “ridges” appeared on the blowby map indicating ring collapse.

As axial width is increased, the flow path through the piston groove is reduced. Reducing the flow path, reduces the blowby passing behind the piston groove. If the flow path between the groove and the ring is reduced too much, the pressure drop across the top of the ring leads to ring collapse.

As mentioned in Heading 5.6, the ring tension is increased as axial thickness increases. Ring tension is a relatively insignificant factor in preventing ring collapse, but increased ring tension is known to accelerate ring wear. Although the ring tension is only increased slightly by altering the axial width, it possesses a slight adverse effect on ring lifespan.

Another undesirable side-effect of increasing the ring’s axial width is that the ring’s inertia increases. Increasing a ring’s inertia often increases the probability of ring collapse, as explained in Heading 3.4.

7.5 Groove Height Analysis

Altering the groove height seems similar to altering the axial width in that they both change the axial clearance. Unlike varying the axial width, varying groove height does not change the ring's inertia. Varying the groove height changes the crevice volume behind the ring and of the adjacent lands.

According to the blowby maps in Heading 10.2.4, Heading 10.3.4, and Heading 10.4.4, blowby at almost all operating conditions slightly increases as groove height increases. The larger groove height, provides a larger crevice volume for combustion gases to flow into.

Under the operating conditions with ring collapse, the ring collapse peak in the blowby maps decreases slightly as ring groove height increases. These smaller peaks are an effect of the ring collapse conditions lasting for a shorter duration of time. The larger ring clearance allows for gases to flow behind the ring groove with less pressure drop. Consequently, the support behind the ring from the gases is improved.

The unusual shape of the blowby map shown in Figure 62 is due to ring flutter. In this instance, ring flutter does not cause its characteristic degradation in ring pack sealing performance. The small ring clearance prevents the usual flow of gases behind the ring groove.

7.6 Small Clearance Between Top of Ring and Top of Groove

It is interesting to note that while a small ring clearance by means of a large axial width results in ring collapse, the same ring clearance by means of a small groove height results in improved ring performance. Hence, it is better to design a thin ring with a small ring clearance, than to design a thick ring with a small ring clearance; the latter design has more inertia.

Reducing ring clearance also has the additional advantage of reducing the effects of the piston ring impacting on its groove. The ring momentum becomes less, because the ring has less distance to achieve a state of high kinetic energy. Large piston ring clearances result in ring and groove characteristics as shown in Figure 16.

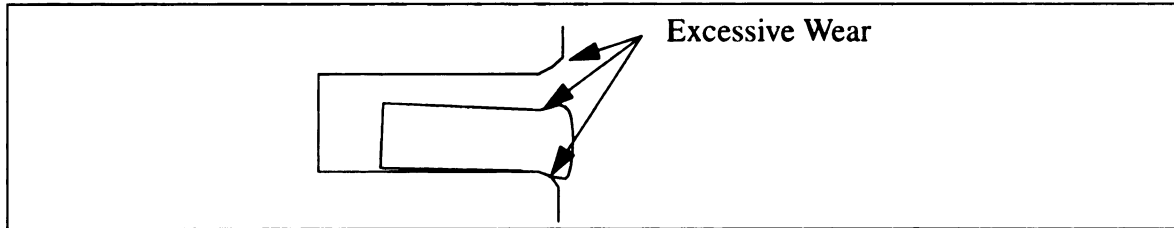


Figure 16: Aged Piston Ring and Groove with Large Clearance

7.7 Radial Thickness Analysis

Heading 10.2.5, Heading 10.3.5 and Heading 10.4.5 suggest that increased radial thickness significantly improves ring sealing performance. The increased radial thickness reduces the crevice volume behind the compression ring. Thus, the amount of combustion gases that can be trapped behind the ring is reduced. Furthermore, if the ring has a relatively small clearance between the inner ring diameter and the inner groove diameter, the ring is prevented from fully collapsing under the ring collapse conditions.

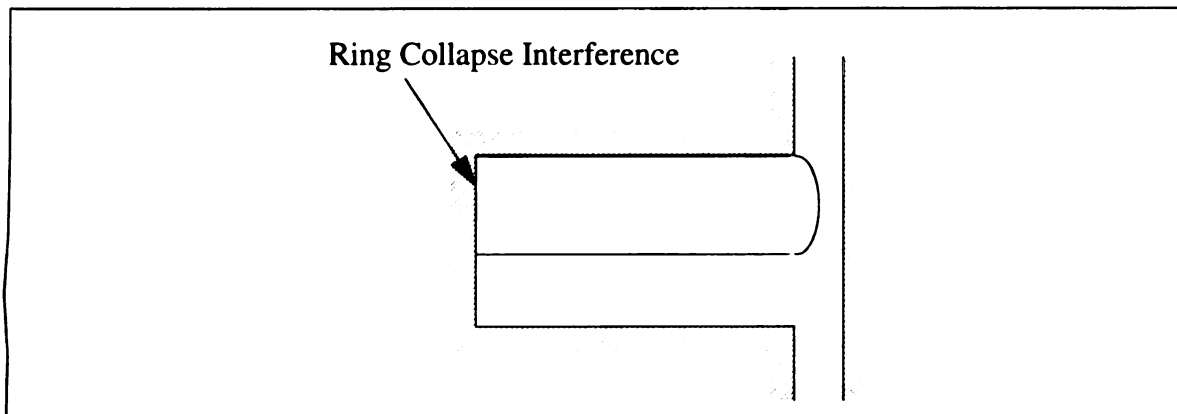


Figure 17: Ring Collapse Interference

Other than slightly increasing ring material, there is no drawback to having a larger radial thickness. However, radial thickness does have an upper limit. The piston ring radial thickness, when “warm,” must not reduce the clearance behind the ring to zero—otherwise excessive wear or seizure will occur.

7.7.1 Relating Ring Wear to Radial Thickness

Over the lifetime of a piston ring, its radial thickness begins to decrease due to ring wear. The plots in Heading 10.2.5, Heading 10.3.5 and Heading 10.4.5 each show a close representation of the reverse progression of a ring performing as it ages. The ring wear simulation would be better if the minor increase in end gap were taken into account.

7.8 Groove Diameter Analysis

7.8.1 Basic Overview

The figures in Heading 10.2.6, Heading 10.3.6, and Heading 10.4.6 show that blowby was reduced as groove diameter increases for all operating conditions with the exceptions of Figure 117 and Figure 118.

The cause of the sealing improvement is similar to the cause explained in Heading 7.5. That is, the smaller crevice volume restricts flow behind the top compression ring. However, the change in performance differs in the two following ways: increasing the groove diameter, makes the groove more shallow; changing the groove diameter does not affect the ring mass.

7.8.2 Exceptions to the Rule

As the groove diameter increases, the ring grooves become more shallow. Consequently, the flow path behind the groove is shorter. A shorter flow path makes it easier for gases to flow behind the ring if the ring flutters. In both Figure 117 and

Figure 118 where ring collapse is detected, the top ring is observed to drop partially in its groove, momentarily following spark. During this dip (see Figure 18), gas easily flows

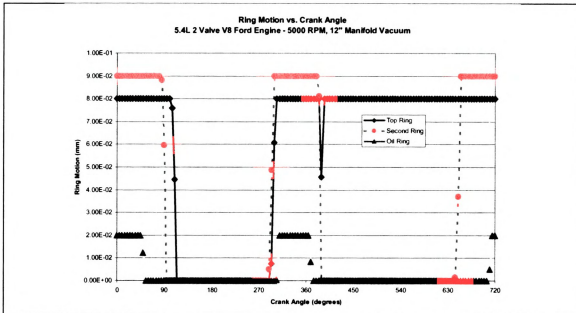


Figure 18: Ring Motion Versus Crank Angle (Ring Collapse) With Top Ring Dip

past the top ring. Since the second ring is sealing better than the top ring during the dip, the land between the top and second ring becomes pressurized. The top ring returns to the top of its groove, resulting in ring collapse during the power stroke.

Where ring stability is not a significant issue, groove diameter can be increased until the ring clearance behind the ring is approximately 0.2 mm for automotive gasoline engines. However, if a ring pack is known to have stability problems, the ring clearance should not be smaller than 0.4 mm in automotive gasoline engine applications.

CHAPTER 8. CONCLUSIONS AND RECOMMENDATIONS

8.1 General Implications

The results from the study performed, indicate that blowby performance follows a predictable continuous pattern with respect to cylinder kit geometries. For improvement in blowby performance, geometric parameters can be increased or decreased until either physical constraints are reached or the ring pack becomes unstable. The ring pack is considered to be unstable when ring collapse is detected. Thus, advanced optimization algorithms are not essential in finding the ideal cylinder design.

8.2 Top Ring Trends

The following table summarizes the effect on blowby performance of the tested geometric parameters as they are increased.

Table 13: Qualitative Parametric Sensitivity
1 designates highest level of influence
5 designates lowest level of influence

Parameter	Ring Pack Stability	Sealing Performance
Top Ring End Gap Clearance	Decrease - 1	Decrease - 1
Top Ring Axial Width	Decrease - 5	Increase - 5
Top Ring Groove Height	Increase - 3	Decrease - 4
Top Ring Radial Thickness	Increase - 4	Increase - 3
Top Ring Groove Diameter	Decrease - 2	Increase - 2

To improve ring pack performance without penalty, end gap clearance should be minimized and radial thickness of the top ring should be maximized. If ring pack stability is not a significant issue with a particular ring pack, the successive design should maximize top ring axial width and groove diameter, while minimizing top ring groove

height. However, if ring pack stability is problematic, those parameters should be altered in the way opposing the preceding statement.

8.3 HC Emissions

While this study did not focus on HC emissions in ring pack design, the reduction of HC emissions are indirectly accounted for in backflow; backflow is a subcomponent of blowby. Therefore, reducing blowby also lowers HC emissions.

It should be noted that, under normal engine operating conditions, one of the largest sources of HC emissions comes from crevice volumes. [15] Increasing radial thickness and groove diameter reduces crevice volumes, and thus decreases HC emissions.

8.4 Top and Second Compression Ring Relation

According to the simulation performed on Ford Motor Company's 5.4 L V8 engine, the second compression ring has a strong effect on ring pack stability. If the second ring seals better than the top ring, pressure builds between the top and second compression ring. This pressure increases the likelihood of ring collapse. Ring collapse conditions can be alleviated by either improving the top ring's sealing performance, or decreasing the second ring's sealing performance.

8.5 Recommendations

The trends summarized in Heading 8.2 shall prove to be useful to piston and ring pack designers. The by-product tool (coded for this study) that automates the simulation over 100 operating conditions should be useful for future studies of other ring pack geometries.

Ring twist was neglected in this study because both the software and hardware technology were currently unavailable. While the CASE system offers a ring twist

analysis program, it cannot automatically generate a finite element grid. To perform such a study in a feasible amount of time, a program that automates finite element gridding would have to be coded. Furthermore on modern computers, stiffness matrices can take up to two hours to generate for each ring pack.

In the future—when faster computers are less expensive—it will be economically and temporally feasible to include ring twist analysis in investigations similar to the one performed in this thesis. Research including ring twist will allow for the accurate parametric studies of cylinder kit geometries' effect on ring wear. Blowby predictions will also better approximate measured blowby values with the implementation of ring twist into cylinder kit parametric experiments.

Although the CASE system simulation has proved to be an accurate predictor of cylinder kit performance, the results require physical testing for absolute confirmation. Future efforts should be made to verify some of the piston ring configuration performances analyzed in this study.

CHAPTER 9. REFERENCES

1. Total Seal. Ring Flutter. [Online Available]
<http://www.totalseal.com/flutter.html>, July 9, 2000.
2. Thompson, N. D. and Wallace, J. S., "Effect of Engine Operating Variables and Piston and Ring Parameters on Crevice Hydrocarbon Emissions," SAE paper 940480, 1994.
3. Kuo, T., Sellnau, M. C., Theobald, M. A. and Jones, J. D., "Calculation of Flow in the Piston-Cylinder-Ring Crevices of a Homogeneous-Charge Engine and Comparison with Experiment," SAE paper 890838, 1989.
4. Ellerman, J., Rohrl, and M. D., Schelling, H., "Oil Consumption and Blowby of Truck Diesel Engines—Test Bench Results," SAE paper 810937, 1981.
5. Mid-Michigan Research, "CASE Theoretical Manual," Mid-Michigan Research, 1998.
6. Ejakov, M. A., Schock, H. J., Brombolich L. J., Carlstrom, C. M. and Williams, R. L., "Simulation Analysis of Inter-Ring Gas Pressure and Ring Dynamics and Their Effect on Blow-by," ASME paper 97-ICE-50, 1997.
7. Yun, J. E., Chung, Y., Chun, S. M., and Lee, K. Y., "Study of a Piston Ring Assembly Design through Experimental and Numerical Investigation of Inter-Ring Gas Pressure and Blowby in a Four-Stroke SI Engine," SAE paper 958524, 1995.
8. Heywood, J. B., "Internal Combustion Engine Fundamentals," McGraw-Hill, Inc., 1988.
9. Truscott, R. T., Reid, T. and Ruddy, B., "Ring Dynamics in a Diesel Engine and Its Effect on Oil Consumption and Blowby," SAE paper 831282, 1983.
10. Cengel, Y. A. and Boles, M. A., "Thermodynamics an Engineering Approach," Third Edition, McGraw-Hill, Inc., 1998.
11. Cook, C. L., Power Piston Ring Performance. [Online Available]
<http://www.tfhudgins.com/cook/faq/faq3.html>, March 19, 1997.
12. Wentworth, J. T., "Effect of Top Compression Ring Profile on Oil Consumption and Blowby with the Sealed Ring-Orifice Design," SAE paper 820089, 1982.
13. Viccino, D., Piston Ring Technology - Sophistication or Necessity. [Online Available]
<http://members.aera.org/EngineTech/edge1296/page3.htm>, June 29, 2000.
14. Federal Mogul., Piston Ring Technology. [Online Available]
http://www.federalmogul.com/products_main/am_underhood/piston_rings_speed_pro.htm, June 29, 2000.
15. Dent, J. C. and Lakshiminarayana, P. A., "A Model for Absorption and Desorption of Fuel Vapor by Cylinder Lubricating Oil Films and Its Contribution to Hydrocarbon Emissions," SAE paper 830652, 1983.

CHAPTER 10. APPENDIX A

10.1 Note About Blowby Scale

The blowby maps shown in the headings below have the same blowby scale for each engine of the same parametric study. The end gap variation map sets have the same scale for the 2.3 L I4, 4.6 L V8 and 5.6 L V8 Ford engines, but a differing scale from the groove height variations map set for these same engines. Due to the size of the plots, it would be difficult to analyze some plots if all of the scales were identical for all of the parametric studies.

10.2 Parametric Study Plots for Ford 2.3 L I4 Engine

The Ford 2.3 L I4 engine parametric study blowby maps are included on the following pages.

All of the geometric dimensions are in millimeters unless otherwise specified. Ring 1 refers to the top compression ring, and Ring 2 refers to the second compression ring.

10.2.1 Original Design

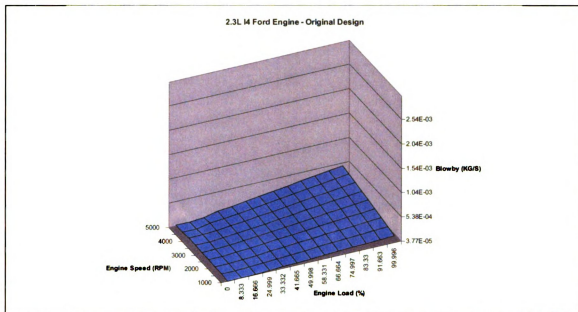


Figure 19: Ford 2.3 L I4 Engine Blowby Map - Original Design

0.305 End Gap Ring 1
 1.476 Axial Width Ring 1
 1.53 Groove Height Ring 1
 3.95 Radial Thickness Ring 1
 86.933 Groove Diameter Ring 1

10.2.2 End Gap Variations

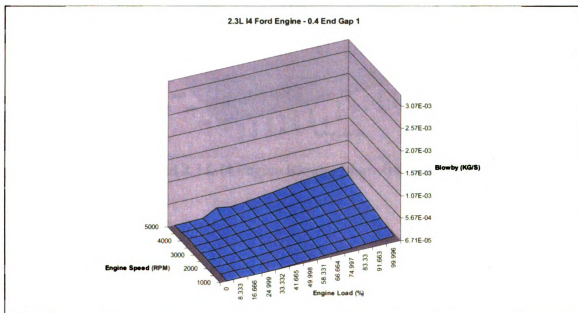


Figure 20: Ford 2.3 L I4 Engine Blowby Map - 0.4 End Gap Ring 1

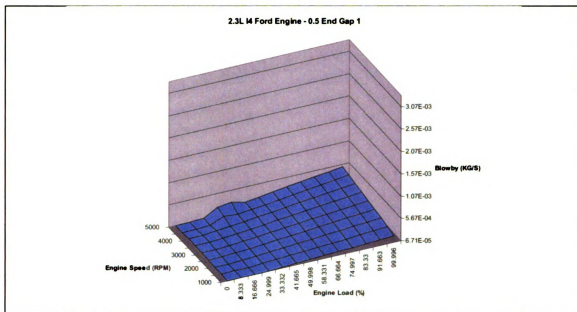


Figure 21: Ford 2.3 L I4 Engine Blowby Map - 0.5 End Gap Ring 1

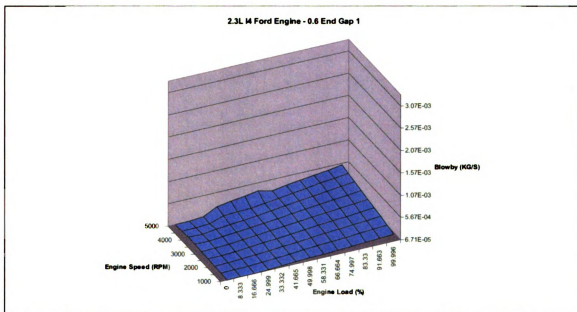


Figure 22: Ford 2.3 L I4 Engine Blowby Map - 0.6 End Gap Ring 1

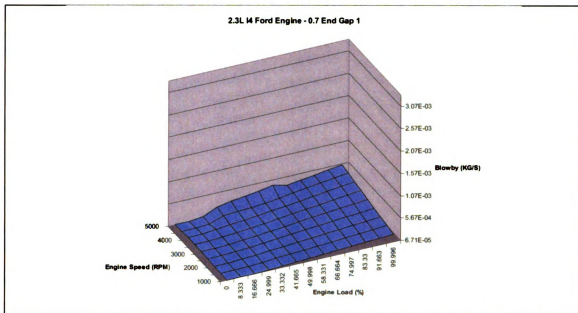


Figure 23: Ford 2.3 L I4 Engine Blowby Map - 0.7 End Gap Ring 1

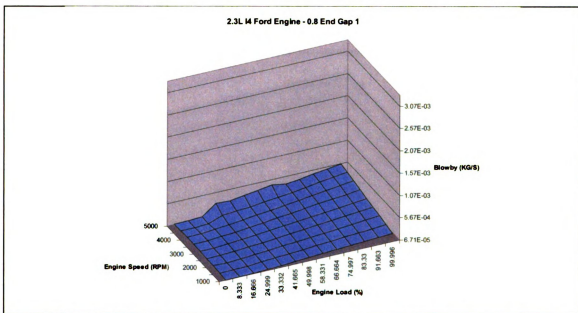


Figure 24: Ford 2.3 L I4 Engine Blowby Map - 0.8 End Gap Ring 1

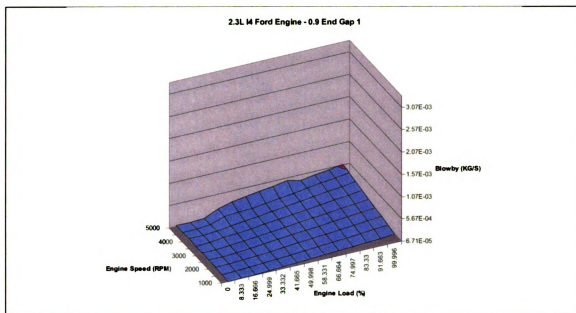


Figure 25: Ford 2.3 L I4 Engine Blowby Map - 0.9 End Gap Ring 1

10.2.3 Axial Width Variations

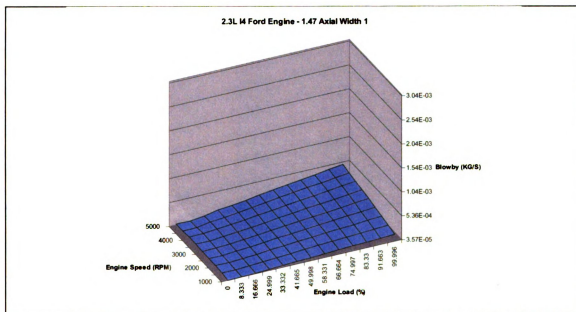


Figure 26: Ford 2.3 L I4 Engine Blowby Map - 1.47 Axial Width Ring 1

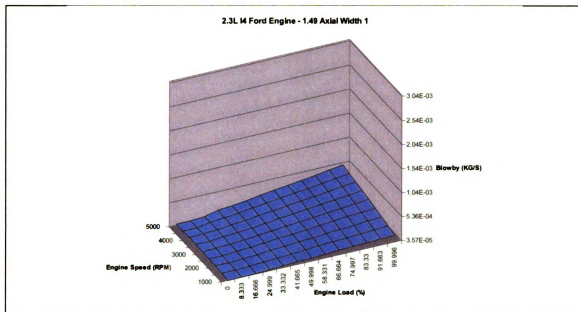


Figure 27: Ford 2.3 L I4 Engine Blowby Map - 1.49 Axial Width Ring 1

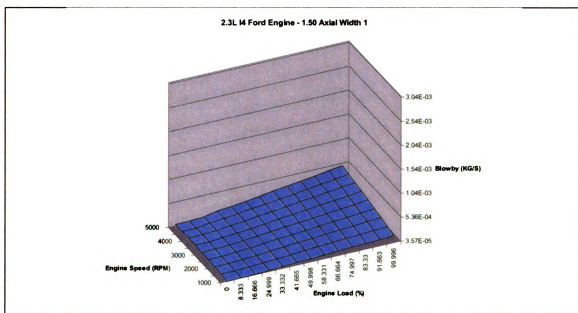


Figure 28: Ford 2.3 L I4 Engine Blowby Map - 1.50 Axial Width Ring 1

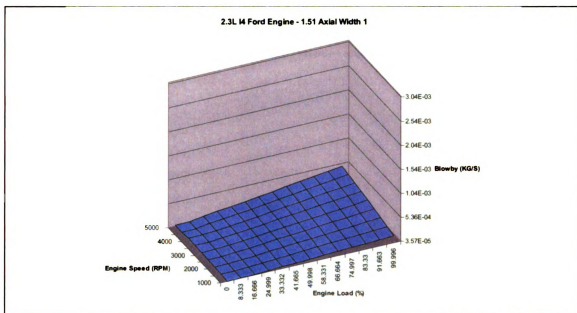


Figure 29: Ford 2.3 L I4 Engine Blowby Map - 1.51 Axial Width Ring 1

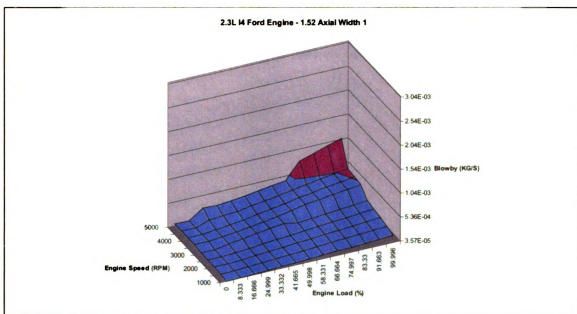


Figure 30: Ford 2.3 L I4 Engine Blowby Map - 1.52 Axial Width Ring 1

10.2.4 Groove Height Variations

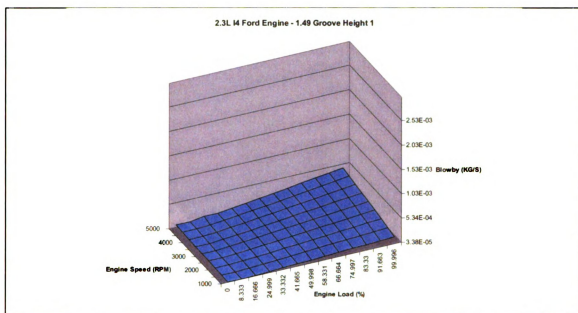


Figure 31: Ford 2.3 L I4 Engine Blowby Map - 1.49 Groove Height Ring 1

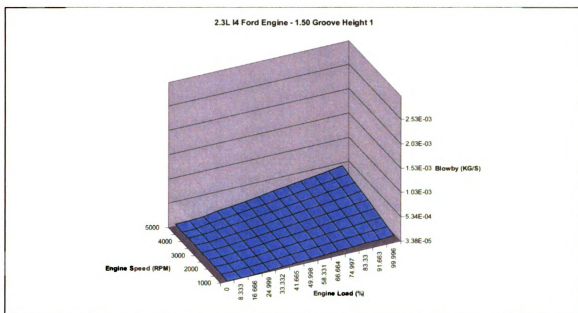


Figure 32: Ford 2.3 L I4 Engine Blowby Map - 1.50 Groove Height Ring 1

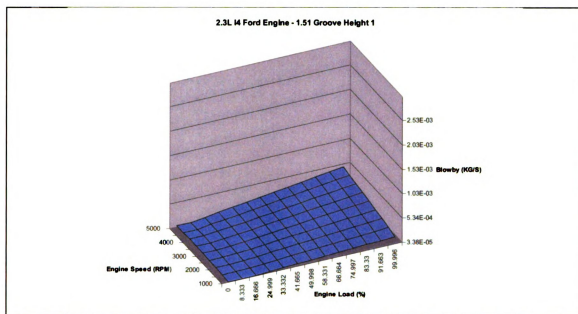


Figure 33: Ford 2.3 L I4 Engine Blowby Map - 1.51 Groove Height Ring 1

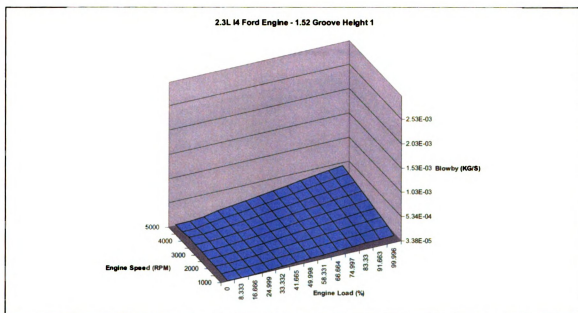


Figure 34: Ford 2.3 L I4 Engine Blowby Map - 1.52 Groove Height Ring 1

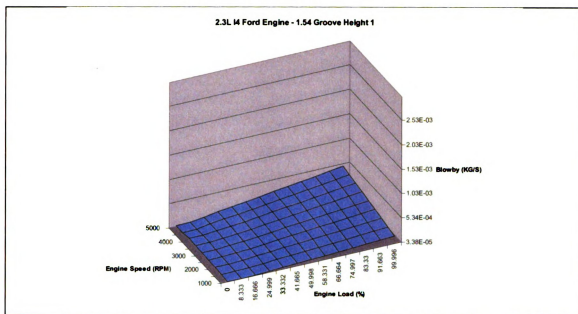


Figure 35: Ford 2.3 L I4 Engine Blowby Map - 1.54 Groove Height Ring 1

10.2.5 Radial Thickness Variations

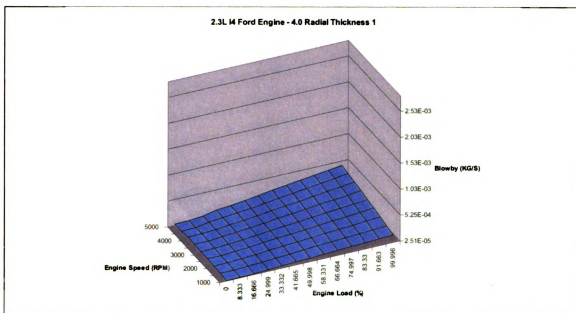


Figure 36: Ford 2.3 L I4 Engine Blowby Map - 4.0 Radial Thickness Ring 1

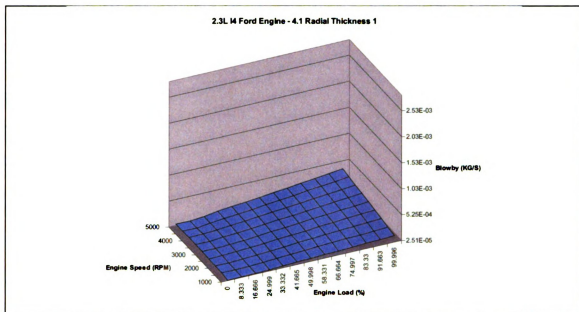


Figure 37: Ford 2.3 L I4 Engine Blowby Map - 4.1 Radial Thickness Ring 1

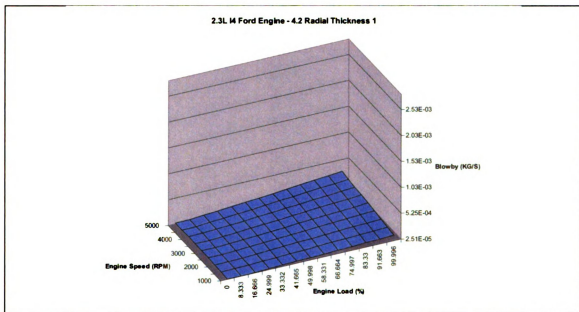


Figure 38: Ford 2.3 L I4 Engine Blowby Map - 4.2 Radial Thickness Ring 1

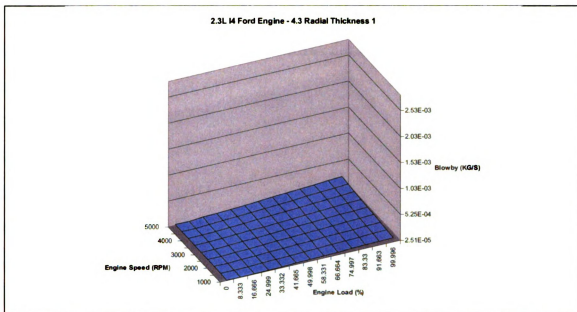


Figure 39: Ford 2.3 L I4 Engine Blowby Map - 4.3 Radial Thickness Ring 1

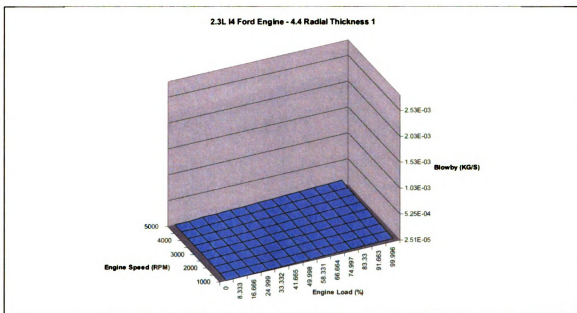


Figure 40: Ford 2.3 L I4 Engine Blowby Map - 4.4 Radial Thickness Ring 1

10.2.6 Groove Diameter Variations

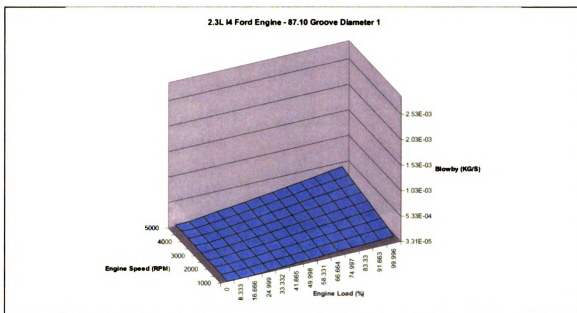


Figure 41: Ford 2.3 L I4 Engine Blowby Map - 87.10 Groove Diameter Ring 1

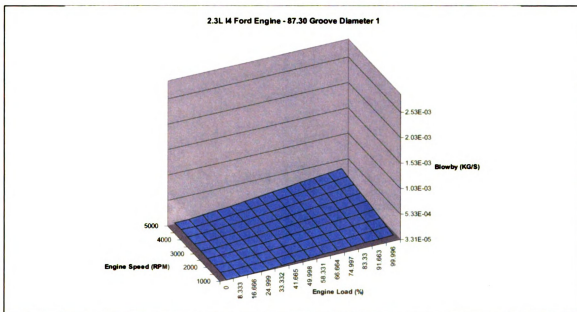


Figure 42: Ford 2.3 L I4 Engine Blowby Map - 87.30 Groove Diameter Ring 1

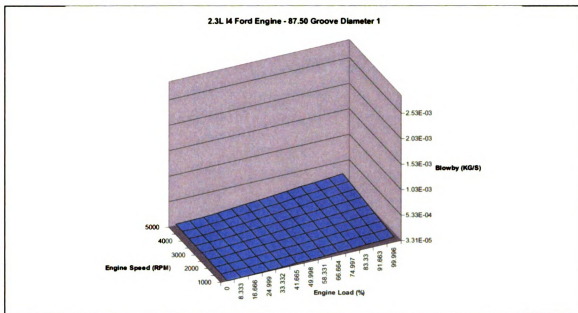


Figure 43: Ford 2.3 L I4 Engine Blowby Map - 87.50 Groove Diameter Ring 1

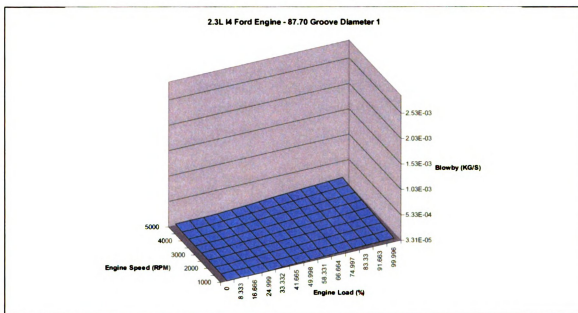


Figure 44: Ford 2.3 L I4 Engine Blowby Map - 87.70 Groove Diameter Ring 1

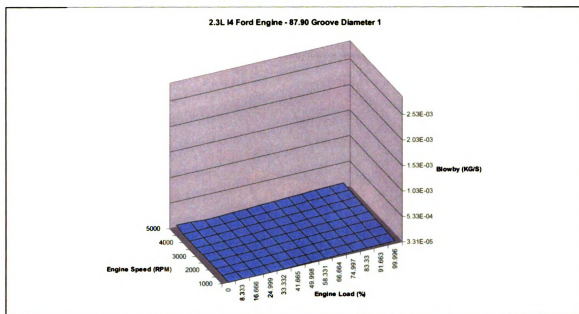


Figure 45: Ford 2.3 L I4 Engine Blowby Map - 87.90 Groove Diameter Ring 1

10.3 Parametric Study Plots for Ford 4.6 L V8 Engine

The Ford 4.6 L V8 engine parametric study blowby maps are included on the following pages.

10.3.1 Original Design

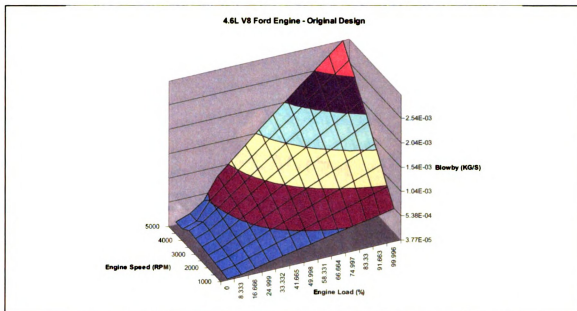


Figure 46: Ford 4.6 L V8 Engine Blowby Map - Original Design
 0.356 End Gap Ring 1
 1.470 Axial Width Ring 1
 1.524 Groove Height Ring 1
 3.965 Radial Thickness Ring 1
 80.71 Groove Diameter Ring 1

10.3.2 End Gap Variations

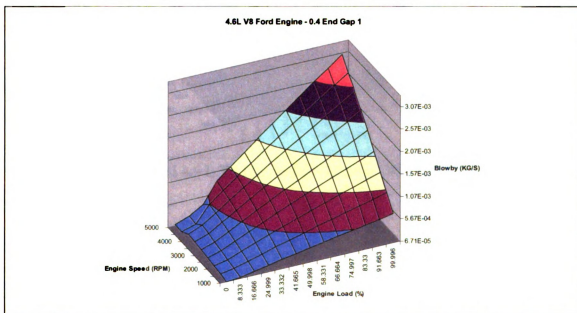


Figure 47: Ford 4.6 L V8 Engine Blowby Map - 0.4 End Gap Ring 1

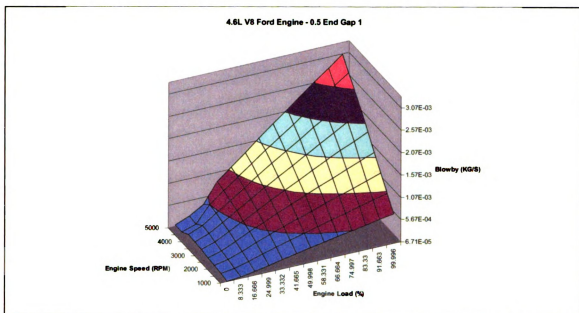


Figure 48: Ford 4.6 L V8 Engine Blowby Map - 0.5 End Gap Ring 1

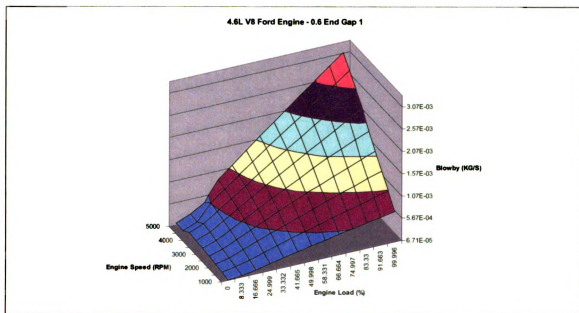


Figure 49: Ford 4.6 L V8 Engine Blowby Map - 0.6 End Gap Ring 1

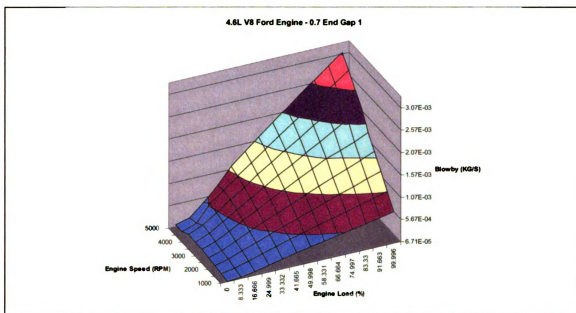


Figure 50: Ford 4.6 L V8 Engine Blowby Map - 0.7 End Gap Ring 1

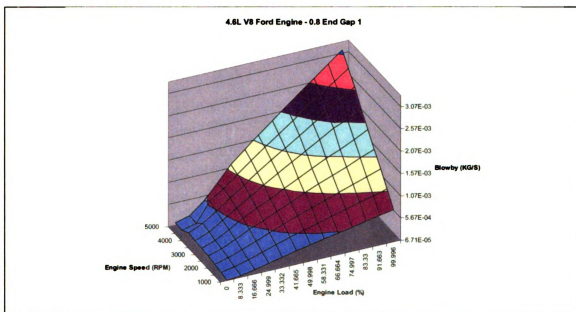


Figure 51: Ford 4.6 L V8 Engine Blowby Map - 0.8 End Gap Ring 1

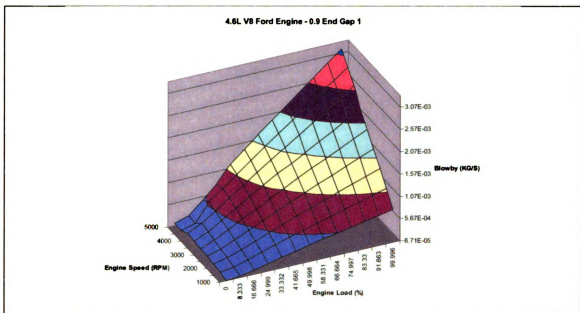


Figure 52: Ford 4.6 L V8 Engine Blowby Map - 0.9 End Gap Ring 1

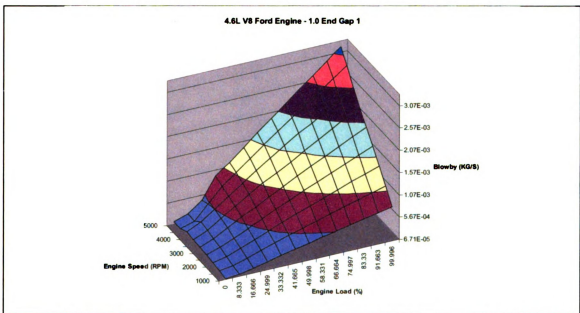


Figure 53: Ford 4.6 L V8 Engine Blowby Map - 1.0 End Gap Ring 1

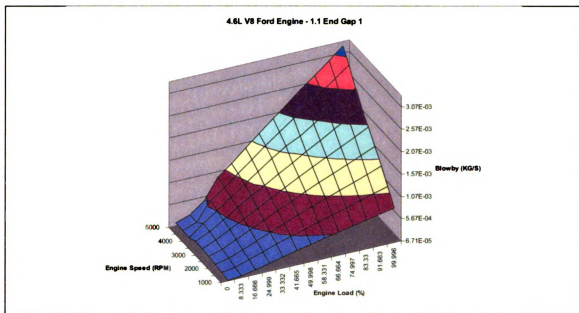


Figure 54: Ford 4.6 L V8 Engine Blowby Map - 1.1 End Gap Ring 1

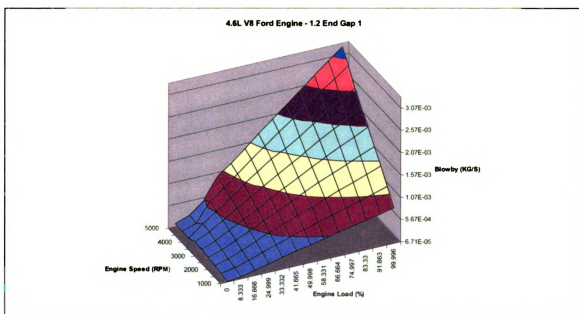


Figure 55: Ford 4.6 L V8 Engine Blowby Map - 1.2 End Gap Ring 1

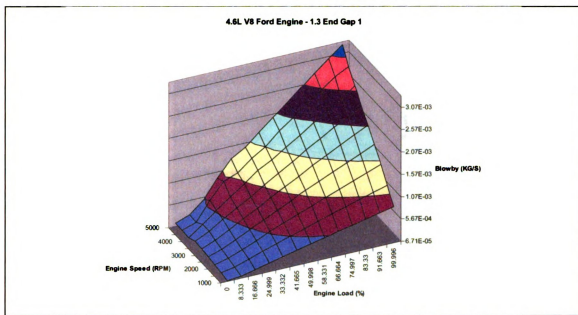


Figure 56: Ford 4.6 L V8 Engine Blowby Map - 1.3 End Gap Ring 1

10.3.3 Axial Width Variation

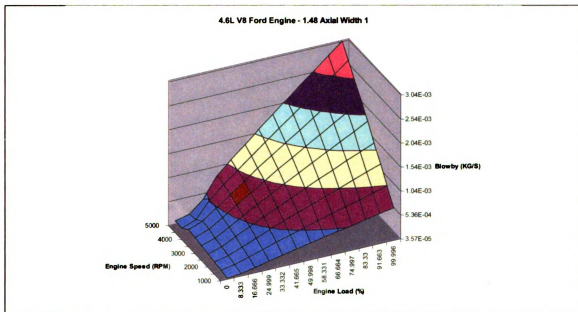


Figure 57: Ford 4.6 L V8 Engine Blowby Map - 1.48 Axial Width Ring 1

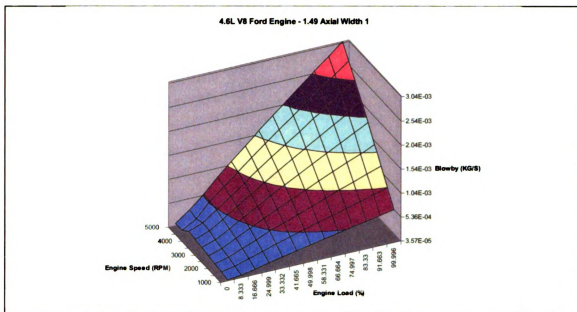


Figure 58: Ford 4.6 L V8 Engine Blowby Map - 1.49 Axial Width Ring 1

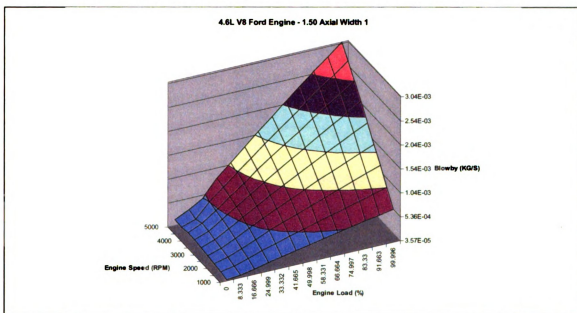


Figure 59: Ford 4.6 L V8 Engine Blowby Map - 1.50 Axial Width Ring 1

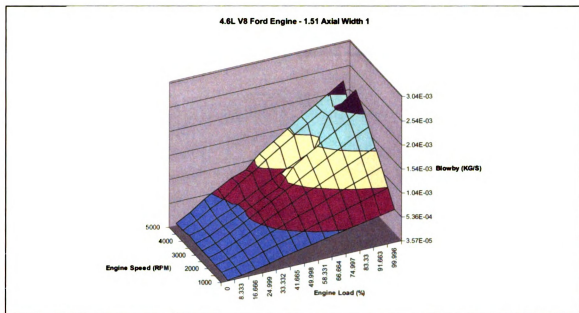


Figure 60: Ford 4.6 L V8 Engine Blowby Map - 1.51 Axial Width Ring 1

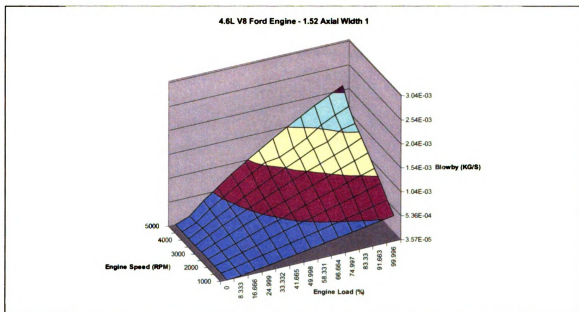


Figure 61: Ford 4.6 L V8 Engine Blowby Map - 1.52 Axial Width Ring 1

10.3.4 Groove Height Variation

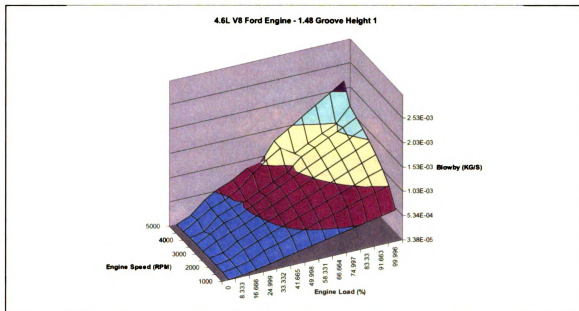


Figure 62: Ford 4.6 L V8 Engine Blowby Map - 1.48 Groove Height Ring 1

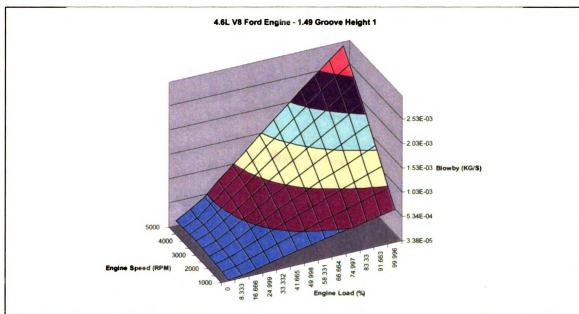


Figure 63: Ford 4.6 L V8 Engine Blowby Map - 1.49 Groove Height Ring 1

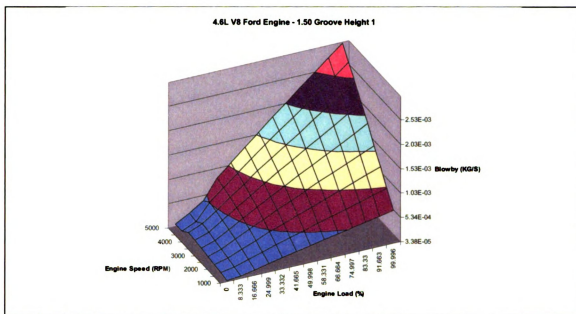


Figure 64: Ford 4.6 L V8 Engine Blowby Map - 1.50 Groove Height Ring 1

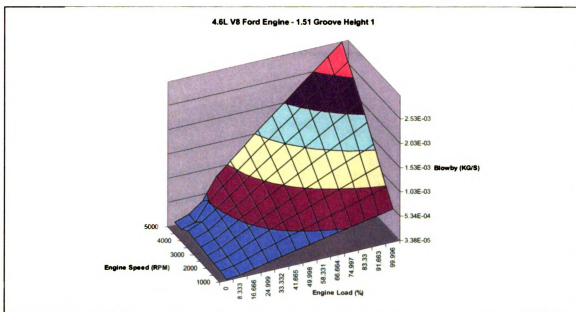


Figure 65: Ford 4.6 L V8 Engine Blowby Map - 1.51 Groove Height Ring 1

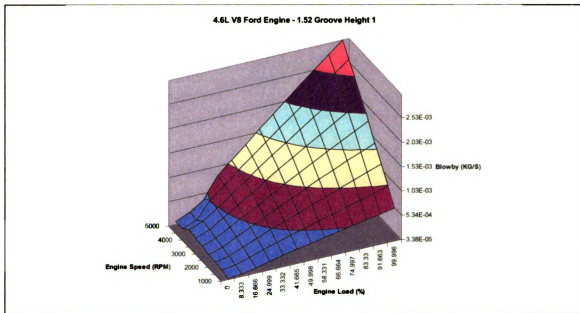


Figure 66: Ford 4.6 L V8 Engine Blowby Map - 1.52 Groove Height Ring 1

10.3.5 Radial Thickness Variations

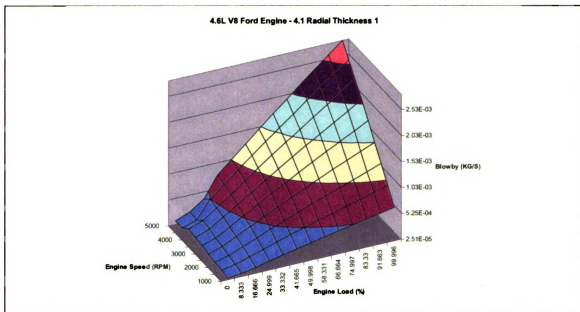


Figure 67: Ford 4.6 L V8 Engine Blowby Map - 4.1 Radial Thickness Ring 1

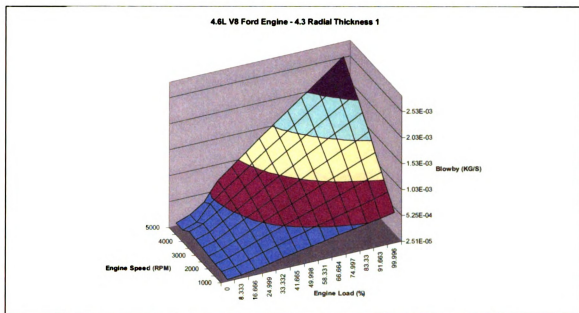


Figure 68: Ford 4.6 L V8 Engine Blowby Map - 4.3 Radial Thickness Ring 1

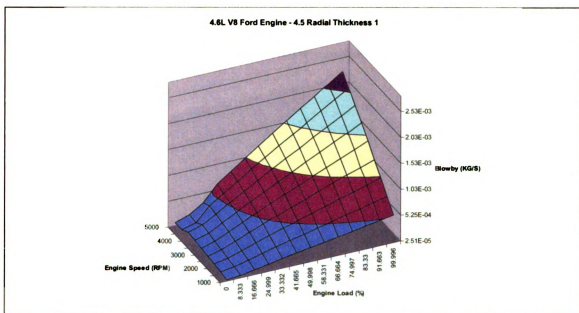


Figure 69: Ford 4.6 L V8 Engine Blowby Map - 4.5 Radial Thickness Ring 1

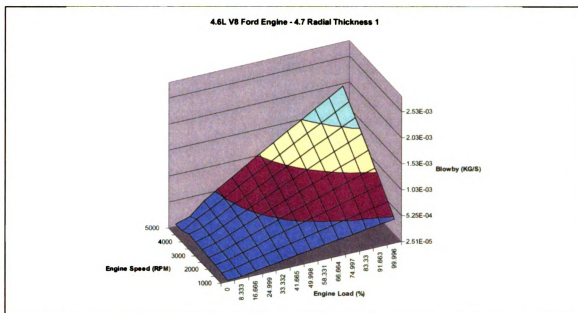


Figure 70: Ford 4.6 L V8 Engine Blowby Map - 4.7 Radial Thickness Ring 1

10.3.6 Groove Diameter Variations

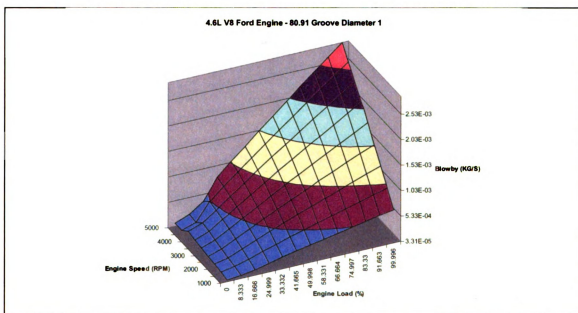


Figure 71: Ford 4.6 L V8 Engine Blowby Map - 80.91 Groove Diameter Ring 1

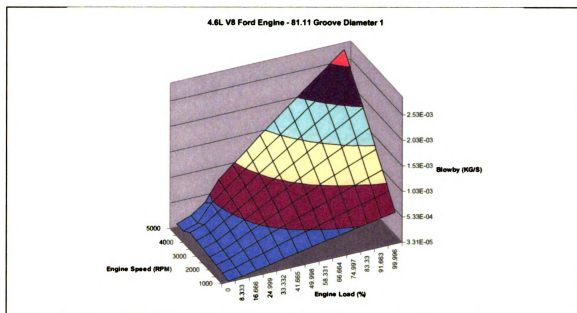


Figure 72: Ford 4.6 L V8 Engine Blowby Map - 81.11 Groove Diameter Ring 1

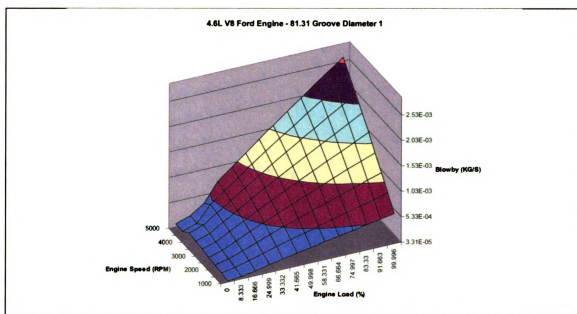


Figure 73: Ford 4.6 L V8 Engine Blowby Map - 81.31 Groove Diameter Ring 1

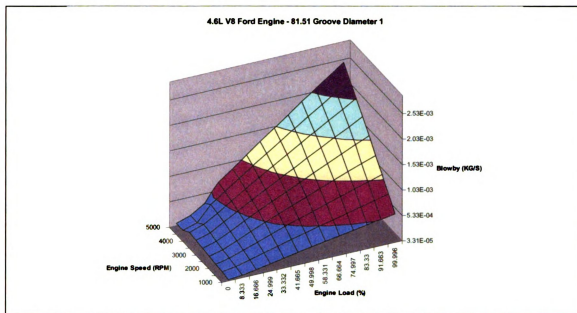


Figure 74: Ford 4.6 L V8 Engine Blowby Map - 81.51 Groove Diameter Ring 1

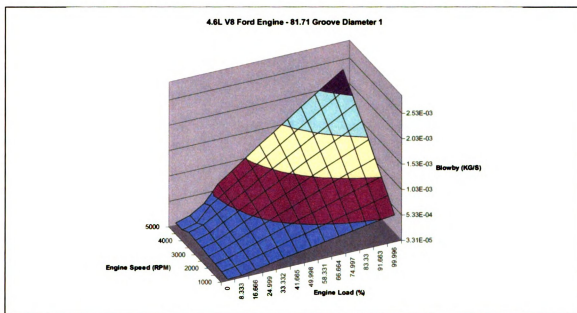


Figure 75: Ford 4.6 L V8 Engine Blowby Map - 81.71 Groove Diameter Ring 1

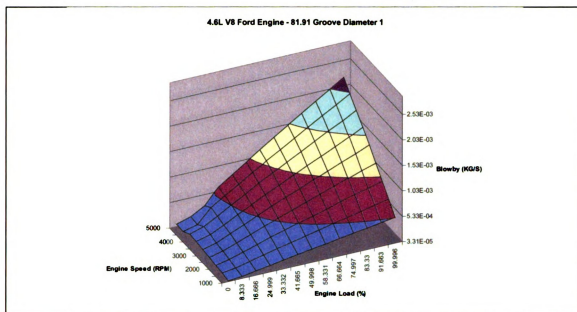


Figure 76: Ford 4.6 L V8 Engine Blowby Map - 81.91 Groove Diameter Ring 1

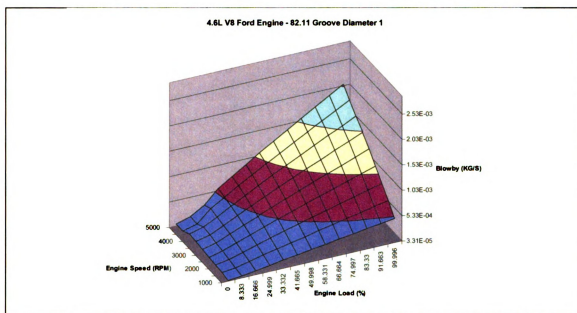


Figure 77: Ford 4.6 L V8 Engine Blowby Map - 82.11 Groove Diameter Ring 1

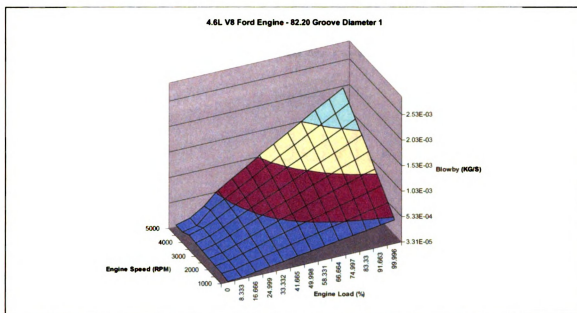


Figure 78: Ford 4.6 L V8 Engine Blowby Map - 82.20 Groove Diameter Ring 1

10.4 Parametric Study Plots for Ford 5.4 L V8 Engine

The Ford 5.4 L V8 engine parametric study blowby maps are included on the following pages.

10.4.1 Original Design

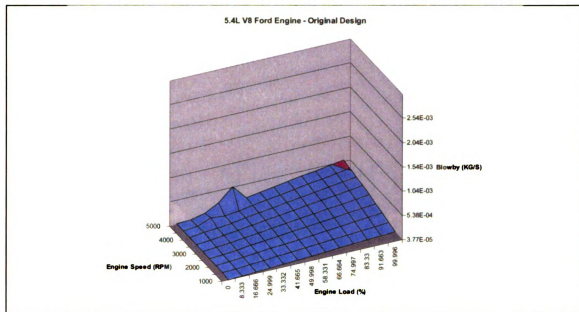


Figure 79: Ford 5.4 L V8 Engine Blowby Map - Original Design

0.356 End Gap Ring 1
 0.356 End Gap Ring 2
 1.45 Axial Width Ring 1
 1.53 Groove Height Ring 1
 3.4 Radial Thickness Ring 1
 82.2 Groove Diameter Ring 1

10.4.2 End Gap Variations

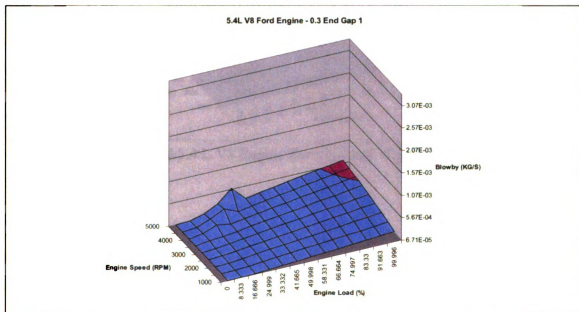


Figure 80: Ford 5.4 L V8 Engine Blowby Map - 0.3 End Gap Ring 1

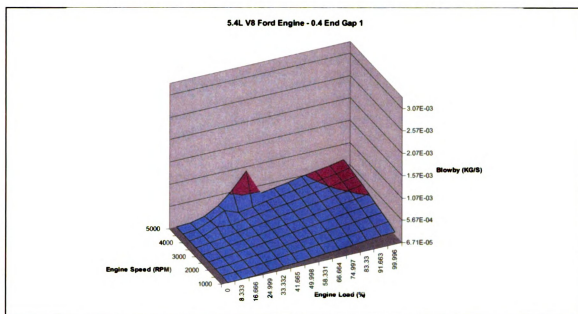


Figure 81: Ford 5.4 L V8 Engine Blowby Map - 0.4 End Gap Ring 1

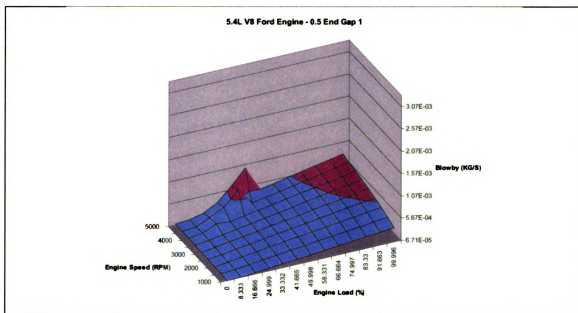


Figure 82: Ford 5.4 L V8 Engine Blowby Map - 0.5 End Gap Ring 1

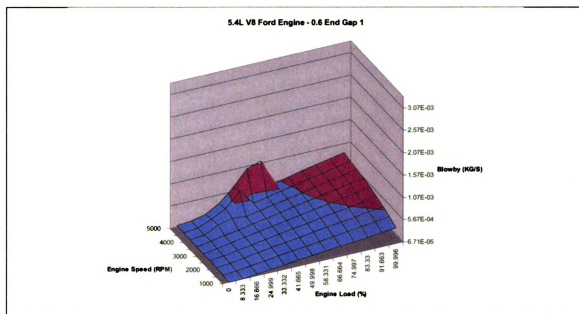


Figure 83: Ford 5.4 L V8 Engine Blowby Map - 0.6 End Gap Ring 1

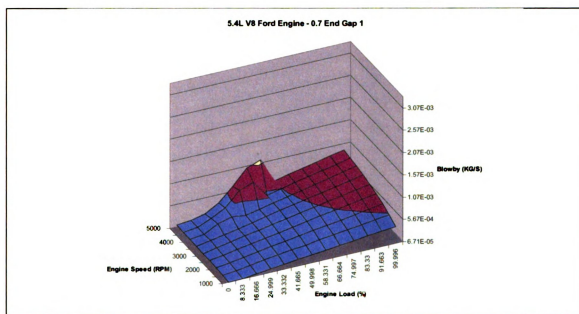


Figure 84: Ford 5.4 L V8 Engine Blowby Map - 0.7 End Gap Ring 1

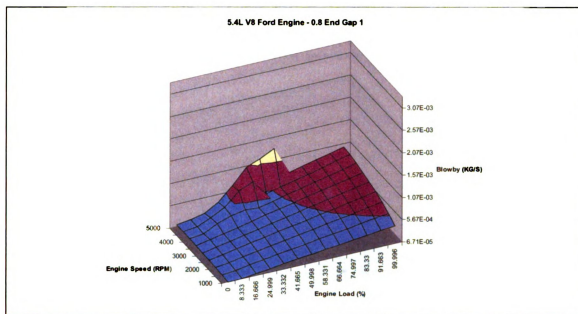


Figure 85: Ford 5.4 L V8 Engine Blowby Map - 0.8 End Gap Ring 1

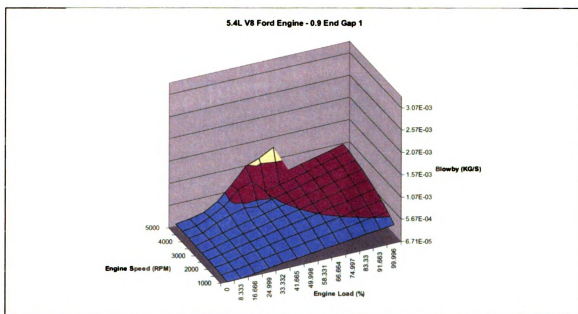


Figure 86: Ford 5.4 L V8 Engine Blowby Map - 0.9 End Gap Ring 1

10.4.3 Axial Width Variations

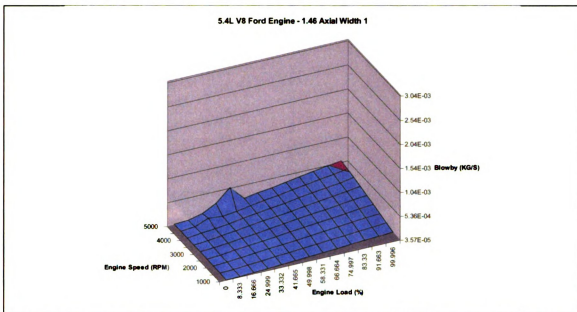


Figure 87: Ford 5.4 L V8 Engine Blowby Map - 1.46 Axial Width Ring 1

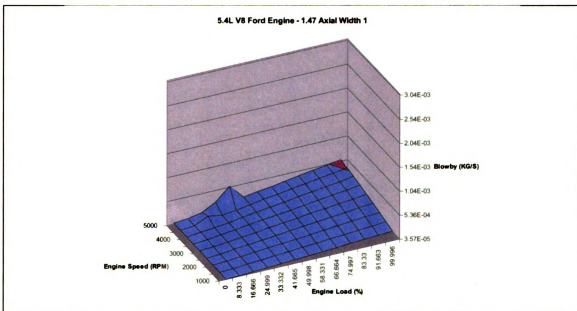


Figure 88: Ford 5.4 L V8 Engine Blowby Map - 1.47 Axial Width Ring 1

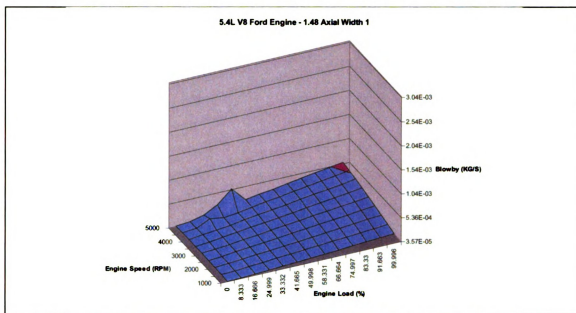


Figure 89: Ford 5.4 L V8 Engine Blowby Map - 1.48 Axial Width Ring 1

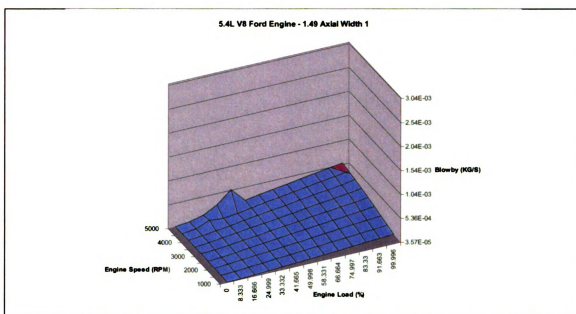


Figure 90: Ford 5.4 L V8 Engine Blowby Map - 1.49 Axial Width Ring 1

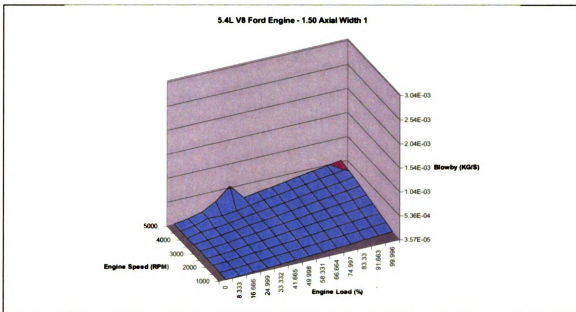


Figure 91: Ford 5.4 L V8 Engine Blowby Map - 1.50 Axial Width Ring 1

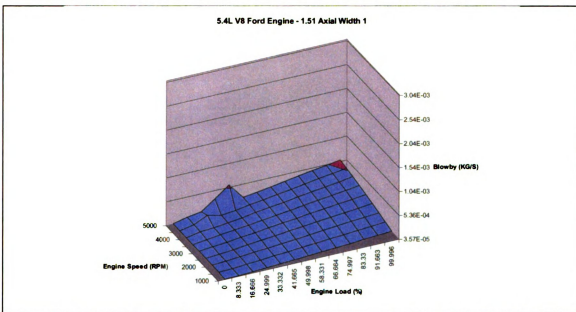


Figure 92: Ford 5.4 L V8 Engine Blowby Map - 1.51 Axial Width Ring 1

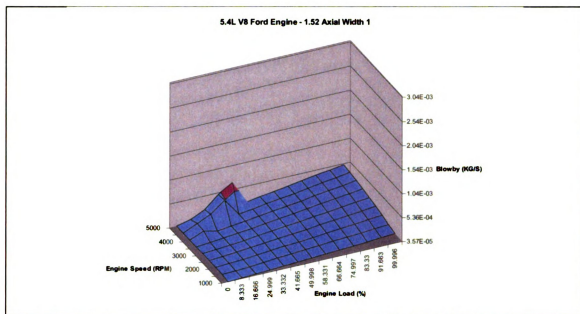


Figure 93: Ford 5.4 L V8 Engine Blowby Map - 1.52 Axial Width Ring 1

10.4.4 Groove Height Variations

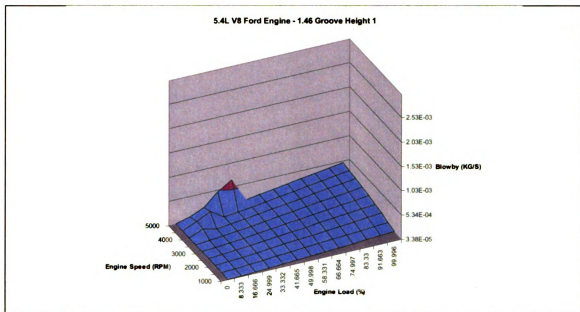


Figure 94: Ford 5.4 L V8 Engine Blowby Map - 1.46 Groove Height Ring 1

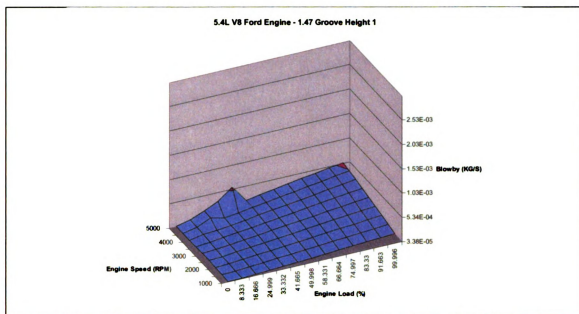


Figure 95: Ford 5.4 L V8 Engine Blowby Map - 1.47 Groove Height Ring 1

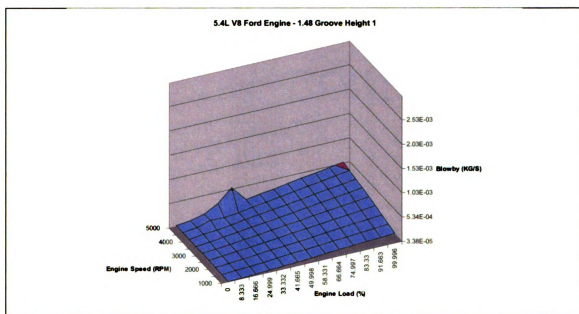


Figure 96: Ford 5.4 L V8 Engine Blowby Map - 1.48 Groove Height Ring 1

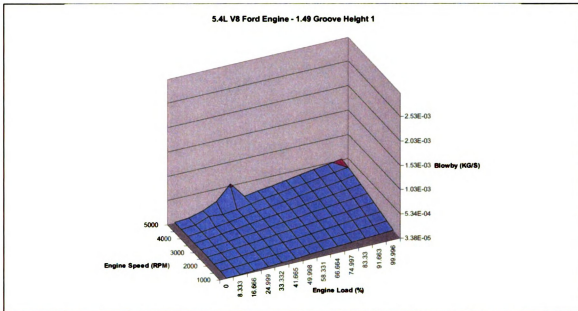


Figure 97: Ford 5.4 L V8 Engine Blowby Map - 1.49 Groove Height Ring 1

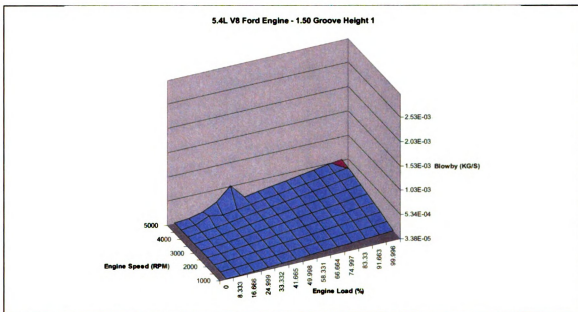


Figure 98: Ford 5.4 L V8 Engine Blowby Map - 1.50 Groove Height Ring 1

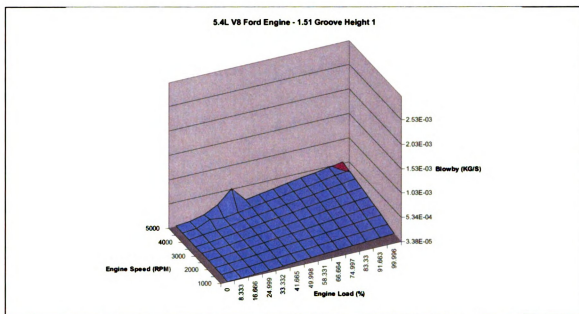


Figure 99: Ford 5.4 L V8 Engine Blowby Map - 1.51 Groove Height Ring 1

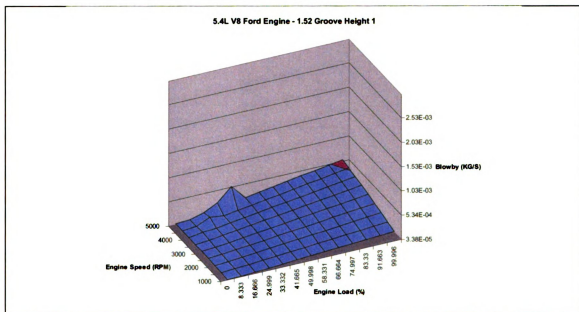


Figure 100: Ford 5.4 L V8 Engine Blowby Map - 1.52 Groove Height Ring 1

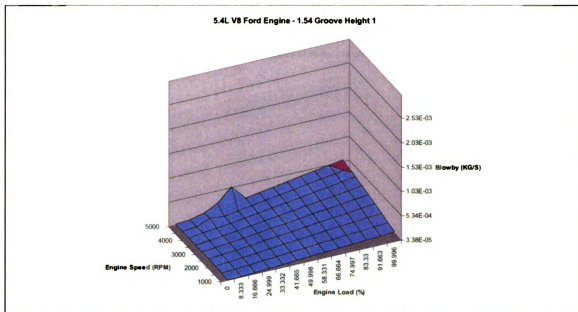


Figure 101: Ford 5.4 L V8 Engine Blowby Map - 1.54 Groove Height Ring 1

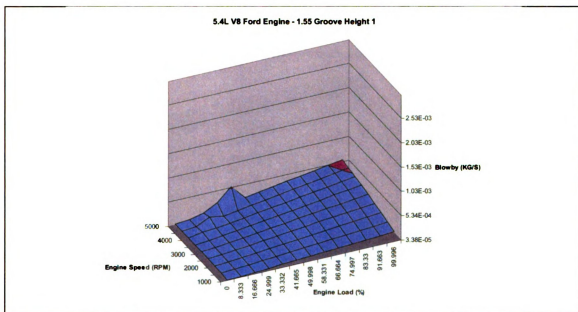


Figure 102: Ford 5.4 L V8 Engine Blowby Map - 1.55 Groove Height Ring 1

10.4.5 Radial Thickness Variations

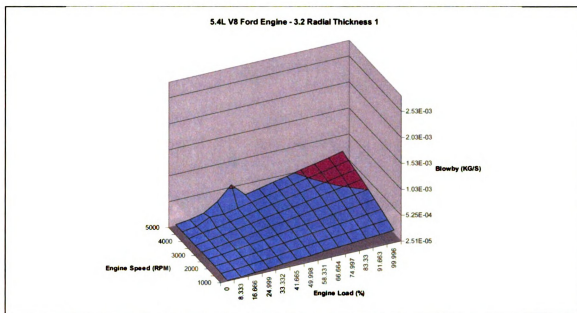


Figure 103: Ford 5.4 L V8 Engine Blowby Map - 3.2 Radial Thickness Ring 1

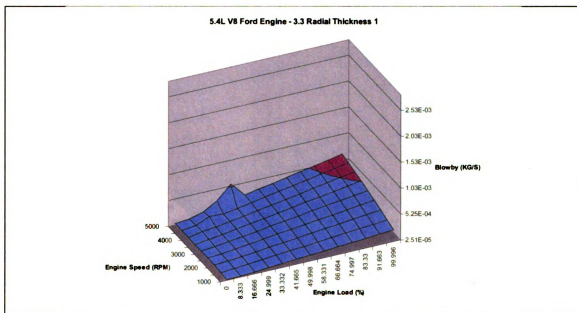


Figure 104: Ford 5.4 L V8 Engine Blowby Map - 3.3 Radial Thickness Ring 1

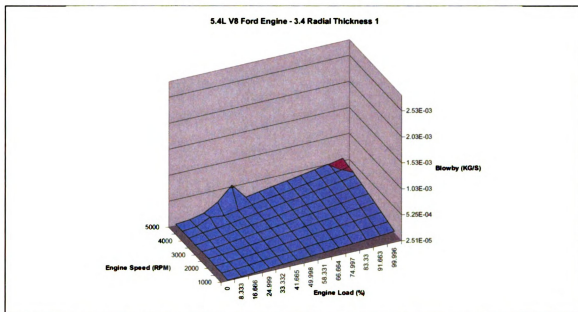


Figure 105: Ford 5.4 L V8 Engine Blowby Map - 3.4 Radial Thickness Ring 1

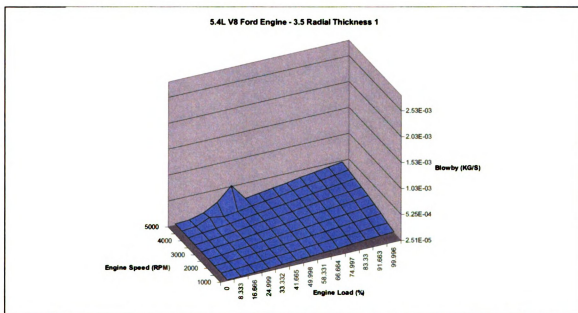


Figure 106: Ford 5.4 L V8 Engine Blowby Map - 3.5 Radial Thickness Ring 1

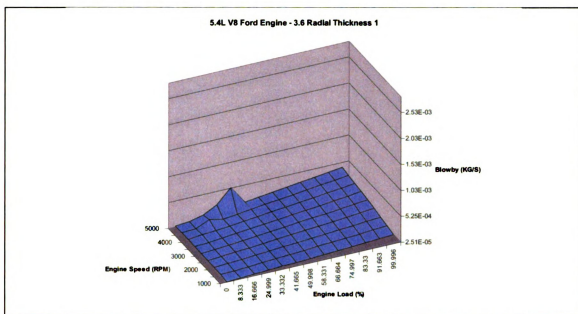


Figure 107: Ford 5.4 L V8 Engine Blowby Map - 3.6 Radial Thickness Ring 1

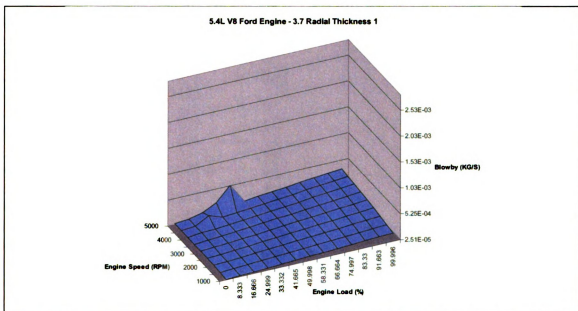


Figure 108: Ford 5.4 L V8 Engine Blowby Map - 3.7 Radial Thickness Ring 1

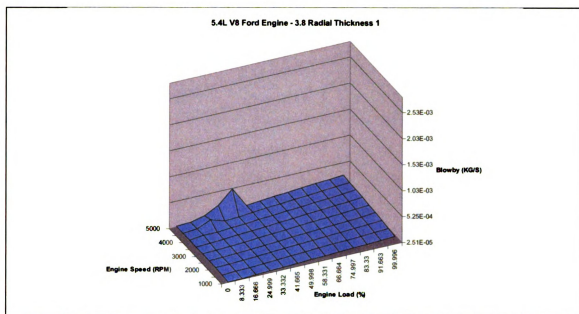


Figure 109: Ford 5.4 L V8 Engine Blowby Map - 3.8 Radial Thickness Ring 1

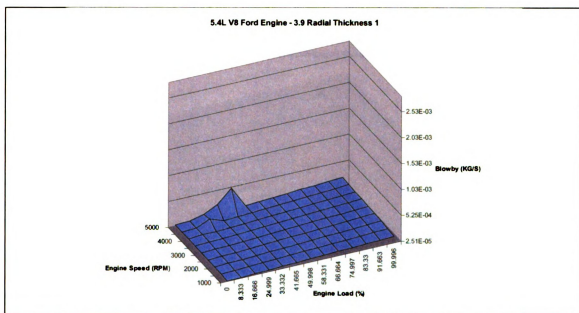


Figure 110: Ford 5.4 L V8 Engine Blowby Map - 3.9 Radial Thickness Ring 1

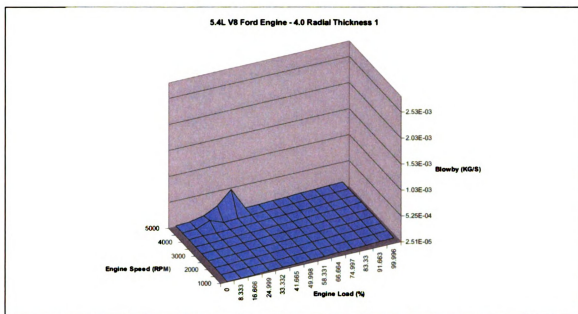


Figure 111: Ford 5.4 L V8 Engine Blowby Map - 4.0 Radial Thickness Ring 1

10.4.6 Groove Diameter Variations

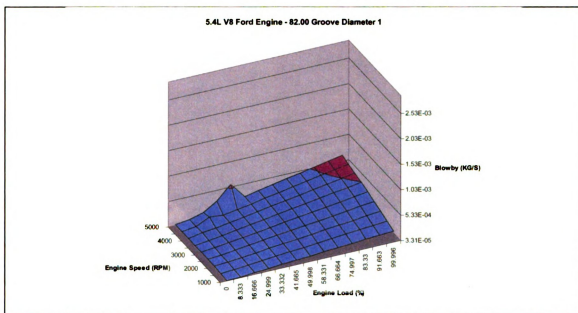


Figure 112: Ford 5.4 L V8 Engine Blowby Map - 82.00 Groove Diameter Ring 1

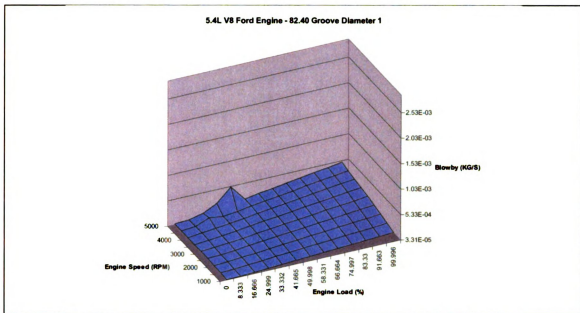


Figure 113: Ford 5.4 L V8 Engine Blowby Map - 82.40 Groove Diameter Ring 1

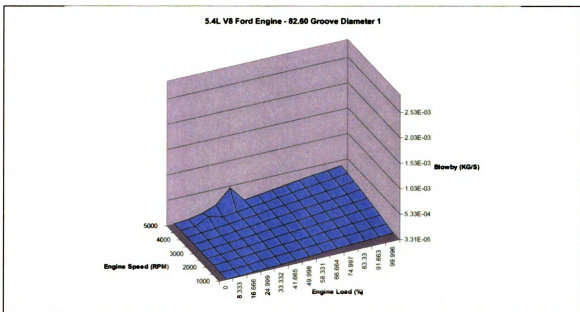


Figure 114: Ford 5.4 L V8 Engine Blowby Map - 82.60 Groove Diameter Ring 1

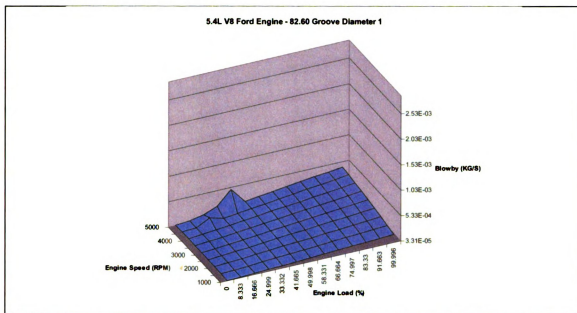


Figure 115: Ford 5.4 L V8 Engine Blowby Map - 82.60 Groove Diameter Ring 1

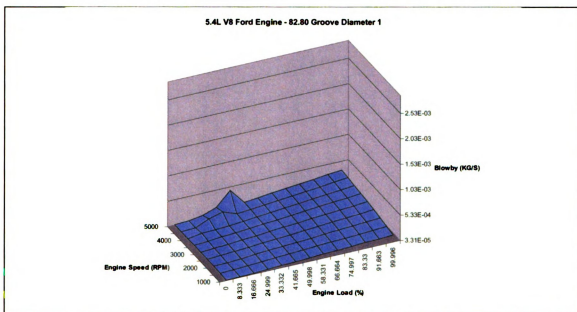


Figure 116: Ford 5.4 L V8 Engine Blowby Map - 82.80 Groove Diameter Ring 1

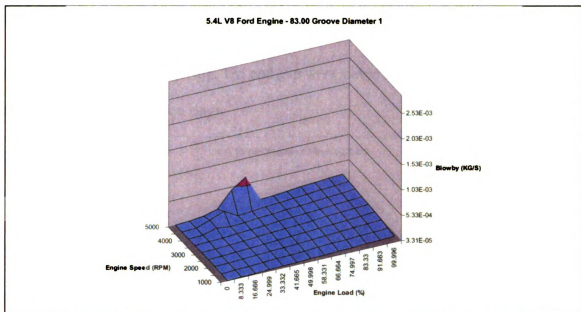


Figure 117: Ford 5.4 L V8 Engine Blowby Map - 83.00 Groove Diameter Ring 1

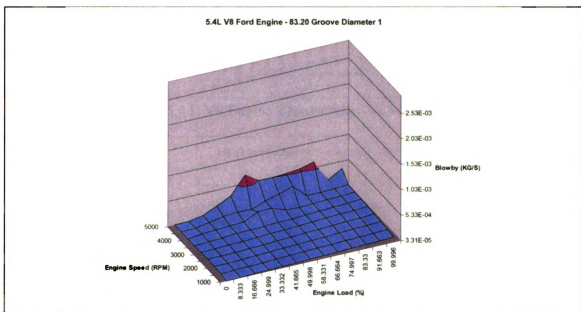


Figure 118: Ford 5.4 L V8 Engine Blowby Map - 83.20 Groove Diameter Ring 1

10.5 Ford 5.4 L V8 Engine Mini-Study

The following blowby maps were used to demonstrate the effect of the second compression ring on the top ring. The end gap were varied in equal quantities for both the top and second compression rings.

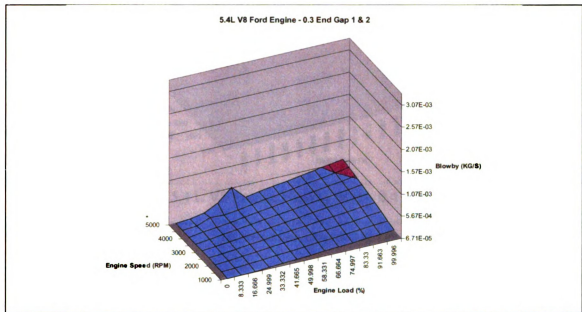


Figure 119: Ford 5.4 L V8 Engine Blowby Map - 0.3 End Gap Ring 1 & 2

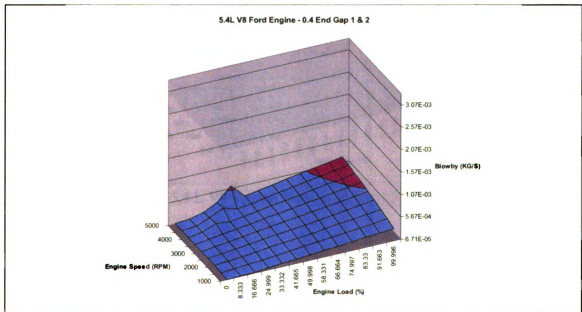


Figure 120: Ford 5.4 L V8 Engine Blowby Map - 0.4 End Gap Ring 1 & 2

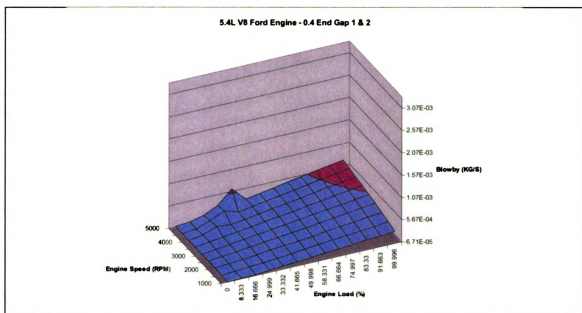


Figure 121: Ford 5.4 L V8 Engine Blowby Map - 0.4 End Gap Ring 1 & 2

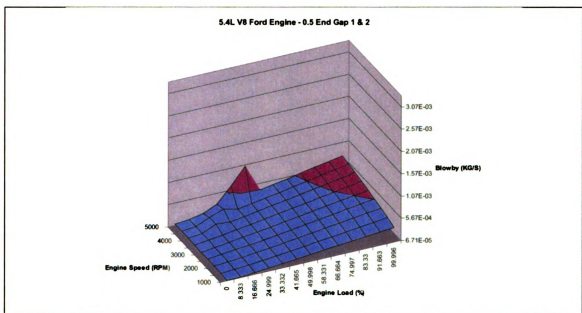


Figure 122: Ford 5.4 L V8 Engine Blowby Map - 0.5 End Gap Ring 1 & 2

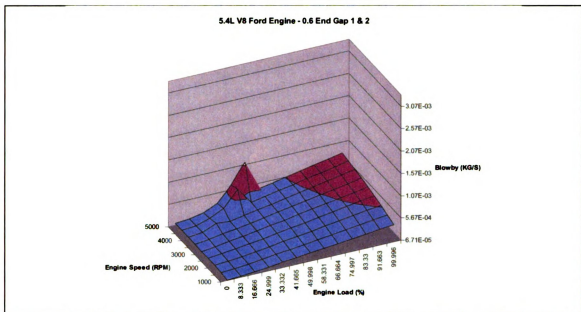


Figure 123: Ford 5.4 L V8 Engine Blowby Map - 0.6 End Gap Ring 1 & 2

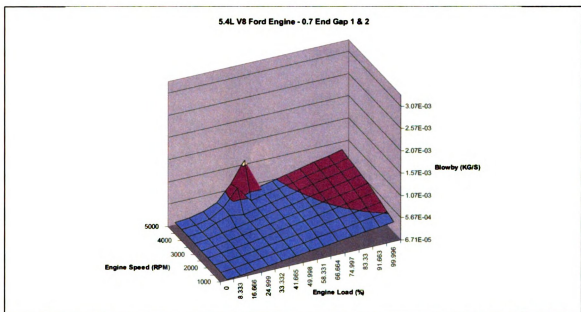


Figure 124: Ford 5.4 L V8 Engine Blowby Map - 0.7 End Gap Ring 1 & 2

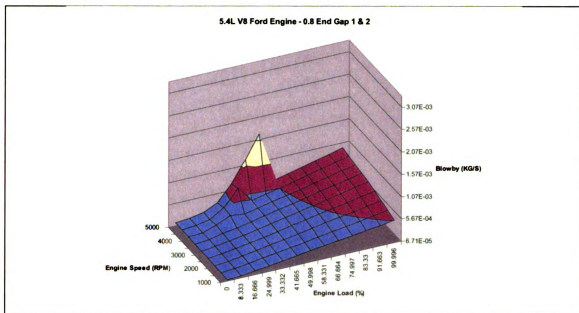


Figure 125: Ford 5.4 L V8 Engine Blowby Map - 0.8 End Gap Ring 1 & 2

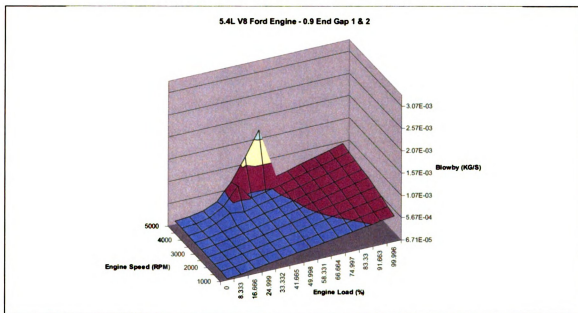


Figure 126: Ford 5.4 L V8 Engine Blowby Map - 0.9 End Gap Ring 1 & 2

MICHIGAN STATE UNIVERSITY LIBRARIES



3 1293 02092 9703